NASA/TM—2016–219164

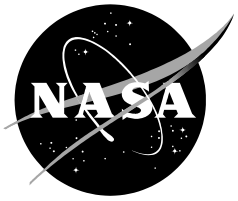

Optimizing Facility Configurations and Operating Conditions for Improved Performance in the NASA Ames EAST 24 Inch Shock Tube

David W. Bogdanoff and
Brett A. Cruden
Analytical Mechanics Associates, Inc.

National Aeronautics and
Space Administration

Ames Research Center
Moffett Field, CA

August 2016

ABSTRACT

The Ames Electric Arc Shock Tube (EAST) is a shock tube wherein the driver gas can be heated by an electric arc discharge. The electrical energy is stored in a 1.2 MJ capacitor bank. Four inch and 24 inch diameter driven tubes are available. The facility is described and the need for testing in the 24 inch tube to better simulate low density NASA mission profiles is discussed. Three test entries, 53, 53B and 59, are discussed. Tests are done with air or Mars gas (95.7% CO_2/2.7% N_2/1.6% Ar) at pressures of 0.01 to 0.14 Torr. Velocities spanned 6.3-9.2 km/s, with a nominal center of 7 km/s. Many facility configurations are studied in an effort to improve data quality. Various driver and driven tube configurations and the use of a buffer section between the driver and the driven tube are studied. Diagnostics include test times, time histories of the shock light pulses and tilts of the shock wave off the plane normal to the tube axis. The report will detail the results of the various trials, give the best configuration/operating conditions found to date and provide recommendations for further improvements. Finally, diaphragm performance is discussed.

I. INTRODUCTION

The Ames Electric Arc Shock Tube (EAST) facility has been used in recent years to simulate radiative heating in flight relevant environments.[1-3] Testing has primarily focused on Earth re-entries[4, 5] and entry to Mars[6-8] in future manned scenarios. The need to decelerate heavy masses in low density atmospheres at Mars have spurred interest in creative solutions to aerodynamic deceleration which will cause heating much higher in the atmosphere than in previous missions. This has prompted much of the work in EAST being driven to lower pressures. Most of the past work with the Ames EAST facility has been done with the 4 inch diameter driven tube. Martian entry tests in the 4 inch tube have been conducted at freestream pressures as low as 0.05 Torr, which corresponds to an altitude of ~50 km. It is found that the success rate of tests in this tube (in terms of useful test time) have been approximately 30%. The 24 inch tube in the EAST facility, also known as the Low Density Shock Tube (LDST) has sat idle for several decades, but offers some potential advantages over the 4 inch tube for these conditions.

In the 1963 study of Mirels, it was shown that theoretical test times in shock tubes should scale as PD^2, where P is freestream pressure and D is the tube diameter.[9] Although Mirels' formulae would put the test time at this condition around 7.6 cm in the 4 inch tube, this length of test time is rarely realized due to departures from ideality in the tube construction, diaphragm breakage and driver initiation. This scaling would suggest that a 24 inch tube could obtain test times 36x larger than the 4 inch tube. Mirels' work also showed that the distance required to obtain maximum test time also scales as PD^2. While this would require an unreasonably long shock tube, the performance gain is non-linear with length. Thus, the 24 inch tube, having its test section 2.7 times further downstream, is estimated to allow a 9.6x improvement in performance, or 73 cm of valid test distance. While this exact number may not be realized, this should translate to greatly improved success rates at the 0.05 Torr condition. At pressures as low as 0.01 Torr, the gain is calculated at 25x, increasing the test distance from 1.6 cm to 41 cm. The tube thus becomes enabling for testing at these low pressures.

A second benefit of the tube is that, at the low light emission levels at lower pressures, the six times longer light integration path of the 24 inch tube could increase the signals by a factor of 6. However, this gain is compromised by a loss in spatial resolution as the optical imaging

cone crosses a longer distance and the spatial resolution is correspondingly reduced. An aperture on the optics is necessary to obtain acceptable spatial resolution, which nearly negates the signal gain due to path length.

Two earlier entries with the EAST 24 inch tube were performed in the 1978 – 1986 time frame. However, these entries had very limited driven tube diagnostics, ionization gauges and pressure transducers only and no spectrometers. High quality spectroscopic diagnostics for the 4 inch driven tube became available in 2008. These spectroscopic diagnostics were implemented in the 24 inch driven tube in 2012. This report describes the characterization of the tube after it was brought back online, and configurational changes that were necessary to obtain acceptable performance.

II. EAST FACILITY DESCRIPTION

The Ames Electric Arc Shock Tube (EAST) is a shock tube wherein the driver gas can be heated by an electric arc discharge. The electrical energy is stored in a 1.2 MJ capacitor bank, which can be configured in 20 kV or 40 kV modes. Figure 1 shows a schematic sketch of the EAST 24 inch tube assembly at the beginning of the first entry discussed in detail herein. Figure 2 shows details of two different conical driver configurations, which will be discussed further below. The driver is typically filled with helium at pressures of 100 – 170 psia. The 4 inch/24 inch driven tube is typically filled with air or Mars gas (95.7% CO_2/2.7% N_2/1.6% Ar) at pressures of 0.01 to 0.14 Torr. A diaphragm separates the driver and driven tubes. The capacitor bank is charged and the discharge is initiated by actuating a pneumatic cylinder which pulls the insulating thread seen in Fig. 2 to the left, bringing the trigger wire (typically stainless steel or tungsten) into contact with the high voltage (HV) electrode. The sudden rise of temperature and pressure upon the arc strike breaks the diaphragm and a shock wave is launched down the driven tube. The shock wave runs down the 4 inch driven tube section, expands out to 24 inch diameter at the cone and continues down the 24 inch tube section to the test section. At the test section, the facility can, for most mission trajectories, match the conditions behind the bow shock in front of a vehicle entering the atmosphere of earth or Mars (for example), allowing radiative heating on the forebodies of these vehicles to be assessed and permitting experimental validation of radiative heating CFD codes.

Data from three entries in the EAST 24 inch shock tube are discussed herein. These are entries 53, 53B and 59, made in the time frame January, 2012 to October, 2015. Each entry consists of multiple runs (typically of the order of 30 to 40) in the facility. Figure 3 is an expanded version of Fig. 1, showing the location of all the diagnostic ports in the tube. At each of stations B, C, E, G, H and J, there are two diagnostic ports facing each other, one located on the east side of the tube and the other on the west side of the tube. Early in the test program, some of these ports contained ionization gauges or photomultiplier tubes (PMTs), while others contained high frequency (0.5 microsecond risetime) piezoelectric pressure transducers (PCB model 132A35). By and large, the pressure transducers proved more informative and reliable than the ionization gauges and PMTs and later in the program, all of these ports were fitted with PCB pressure transducers, with the exception that one PMT was kept at station E. The pressure transducers provide shock velocity data, and, from the difference in the shock arrival time between each pair of transducers, a measure of the horizontal shock tilt across the driven tube. The large ports at A, D, F and I were blanked off and not used except that a pumping station was attached to port F for entries 53B and 59. This pumping station comprised a turbomolecular pump backed by a multi-stage roots pump. The four ports at K are at 45 degrees to the horizontal and three of these ports are fitted with the high speed PCB pressure transducers, while one port is fitted with a PMT (Hamamatsu 1P28) to trigger the spectrometer cameras at station L. With 3 PCB transducers at station K, both the horizontal and vertical shock tilts can be measured at this station. The four ports at station L can be fitted with windows. The window at the west port at L provides light to one or two spectrometers which give spectra of wavelength

versus distance along the tube. (Note that only one spectrometer was used for the first 19 runs of entry 53. All later runs used two spectrometers.) In 4 runs in entry 53, high speed video movies were take through windows on the east side and on the bottom of station L. The cameras used were a Phantom V12.1 at 41,000 frames per second and a Shimadzu HPV-1 at 1 million frames per second. For the last 17 runs of entry 59, a PCB pressure transducer was installed at station L on the east side of the tube.

The diagnostic ports seen in the second and third lengths of the 24 inch tube in Fig. 3 were welded on and produced considerable distortion to the inside surface of the tube at the weld locations. Although the weld distortions ("welts") were ground down to some extent in a tube improvement campaign between Tests 53 and 53B, they could not be completely removed. The first length of the 24 inch tube seen in Fig. 3 has no diagnostic ports and thus, no weld welts. The 3.5 foot long test section is of higher quality than the second and third lengths of the 24 inch tube and appears to be free of weld welts although it contains diagnostic ports.

III. ANALYSIS OF EAST PERFORMANCE

There are two notable causes for unsatisfactory test runs. Typically, the driver gas contamination arrives 2 to 15 cm behind the shock wave, but can arrive almost immediately behind the shock wave. At typical shock velocities of ~7 km/s, 2 to 15 cm correspond to time delays of 3 to 21 microseconds. If contamination arrives at time zero or after only 1 to 2 microseconds, there is no time for the clean flow to even approach equilibrium and the test run must be rejected and repeated. A second cause of unacceptable runs is highly tilted or distorted shock waves. If the shock is sufficiently tilted or distorted, the time histories of the total radiance measured by the spectrometers (i. e., the rise and fall of the total radiance curves), which are integrated across the shock tube, can be badly smeared or distorted (even to the extent of showing two or more peaks). A sample image showing this is given in Figure 4. Despite the similarity in condition between the two tests, the case on the left shows a slow rise in intensity characterized by a separation of over 1 cm from the shock front to the radiation peak and a change of slope, whereas the image on the right is a more expected result where the radiance rises rapidly and cleanly to its peak value then falls according to the different relaxation processes. With distorted or slowly rising total radiance curves, no confidence can be placed in the experimental non-equilibrium peak and the relaxation to equilibrium. This renders such experimental runs useless for CFD code validation. In the following sections, this report details a number of techniques tested out during EAST entries 53, 53B and 59 with a view to improving the performance of the 24 inch driven tube, i.e., to increase the percentage of successful (satisfactory) shots.

IIIA. ENTRY 53

Tests in Mars gas in the 24 inch tube were begun as part of EAST Campaign 53. Figure 2 shows the two conical driver configurations used in this entry. Figure 2(a) shows the trigger wire configuration wherein the main trigger wire is connected to the center of a cross wire which returns to the ground electrode. Figure 2(b) shows the configuration wherein the main trigger wire connects to a ground electrode in which a four-legged "spider" is machined. With the first configuration, part of the arc must run radially (i.e., perpendicular to the tube axis). This results in very large axial j x B (Lorentz) forces on the radial part of the arc. (The current can be of the order of 1 mega-ampere.) The Lorentz forces could accelerate the gas in the radial part of the arc and lead to gas velocities on the order of 20 km/s. Thus, this gas can form driver gas jets which can drive into the driven gas (the test gas), leading to zero or very short contamination

free test time. With the second configuration, ideally, there would be no axial j x B forces. In reality, since the arc will not be perfectly axial in the second configuration, there will be some axial j x B forces even in this case, but one might expect them to be considerably smaller than in the case of the first configuration. Once the wire is destroyed (almost immediately), the arc is free to move around, which should help to average out this j x B force. It is thought that the arc will remain attached to the center pin in the spider configuration, which should result in more repeatable tests and more uniform diaphragm breakage due to the axisymmetric geometry.

The following parameters were used in Entry 53.

Driver gas: helium at 100 – 170 psia
Driver volume: 1292 cm^3
Capacitor bank voltage: 19 – 35 kV
Diaphragms: 0.010" thick 5052-H34 aluminum or 0.012" thick 1100-O aluminum
Driven gas: ~0.05 Torr or ~0.100 Torr Mars gas (95.7% CO_2/2.7% N_2/1.6% Ar) except for run 9, which was 0.011 Torr Mars gas

The nominal conditions were chosen mainly based on an extensive history of mostly successful operation of the EAST facility 4 inch driven tube with these parameter values. The data obtained in the 24 inch tube could then be verified against comparable test data in the 4 inch tube.

Figure 5 shows the test time (free of driver gas contamination) versus run number for entry 53. Figure 6 shows the shock wave tilt time delay versus run number for entry 53. (This time delay is defined as the shock arrival time at the pressure transducer on the east side of the tube minus the shock arrival time at the corresponding transducer on the west side of the tube.) These time delays were measured by pressure transducers at ports 16 cm upstream of the test section (station K). For a representative shock velocity of 7 km/s, the shock tilt angle in degrees is ~0.66 times the shock wave tilt delay time in microseconds. The larger shock tilt angles correspond to strongly tilted and/or distorted shock waves, resulting in unacceptable smearing and distortion of the spectrograms and rendering the measured time histories of the light rise and fall of the shock wave unusable. In Figs. 5 and 6, the terminology "double shock" is used. (In later figures, the terminology "triple shock" is also used.) These terms are used for brevity and refer to shock wave light histories with significant kinks or multiple peaks. They do not necessarily refer to two or three separate shock waves. A sufficiently distorted (wrinkled) shock wave could produce this effect in the light traces, since the photomultiplier tubes integrate the light emission across the tube. It is also possible that a sufficiently tilted shock could produce a significant reflected shock wave on encountering the tube wall. Further discussion of the effect due to tilted/distorted shock wave will be presented at a later point. In general, if the test time is greater than 4 to 8 microseconds (depending on the operating conditions), there is enough time for the light emission to approach equilibrium and the run can be regarded as satisfactory with respect to test time. A run can be regarded as satisfactory with respect to shock wave tilt if the shock wave tilt time delay is less than approximately 1.3 microseconds. However, examination of the shock wave light history is always necessary to determine whether the level of shock wave tilt or distortion is acceptable. The shock wave tilt time delay can be 1.3 microseconds or less and the light history curve can still have unacceptable kinks and/or multiple peaks.

The high speed video measurements taken during Entry 53 have afforded a few shock wave pictures. Figure 7 shows a bottom view of the shock wave in the test section for Entry 53, run 34. A bright region is noted in front of the main shock in the upper part of the picture. The extent of this leading feature corresponds to 6.7 cm, while the tilt at station K corresponds to 9 cm. In contrast, Fig. 8 shows a side view of a nearly planar shock wave in the test section for Entry 53, run 35. The tilt was near zero for run 35. From Fig. 5, the test times were near zero for run 34 and unknown for run 35. However, the picture of Fig. 8 strongly suggests that the driver gas is very close to the shock wave for run 35, and hence, the useful test time would be expected to be very short for run 35, also. Of the shots with camera images, only 2 had simultaneous spectrometer measurement. The correspondence of shock images with

spectrometer traces is shown in Figure 9, where the shock images have been scaled to match the approximate width of the spectral trace. It is noted that the spectrometers may be viewing the shock from slightly different locations than the high speed cameras were, so the correspondence may not be exact. However, the extent of the radiation preceding the main shock in the video frame for run 30 does roughly correspond to that of the light preceding the main peak in the spectrometer trace. This slow rise in radiation may be attributed to a tilt of the shock in the plane perpendicular to the page (through which the camera measures). A tilt in the vertical direction is also apparent in the image. The time of arrival measurements, sampling in a plane midway between these two, measured a tilt time delay of 2 μs, which corresponds to a tilt offset of 1.4 cm over the 60 cm tube diameter. Run 36 shows a narrower light peak on the spectrometer and sharper shock front, relative to run 30. Non-uniformity in the shock front is apparent however, and this is manifested as an inflection in the initial rise in radiance. The measured tilt time of arrival differences were small in this shot, which again demonstrates that a small measured tilt is necessary, but not sufficient, to obtain acceptable data quality.

For the following discussion, we divide the data of Figs. 5 and 6 into five run number groupings, as given below.

Runs 1 - 4: No data
Runs 5 – 21: Cross wire trigger wire configuration
Runs 22 – 33: Spider trigger wire configuration, “good”
Runs 34 – 42: Spider trigger wire configuration, “bad”
Runs 43 – 45: Spider trigger wire configuration, full capacitor bank

Runs 1 to 42 were with “half” capacitor bank (861.3 microfarads), while runs 43 – 45 were with the full capacitor bank (1530 microfarads). Switching from the cross wire configuration (runs 5 – 21) to the “good” spider configuration (runs 22 – 33) produced large improvements in test times and shock wave tilt time delays. The performance of the spider configuration in runs 34 – 42 (“bad”) was inferior to that in runs 22 – 33, but still better than that of the cross wire configuration. It is not known why test performance degraded from runs 22 – 33 to runs 34 – 42; they employed exactly the same physical configuration. One possibility is that wear on the spider electrode due to arc and shock wave impingement reduces its performance over time. The copper electrode tip (see Fig. 2b) is replaced when excessive wear is apparent, typically every 15 to 20 runs. The wear on the remainder of the electrode is less severe, making it difficult to determine whether replacement is required. Due to the cost and complexity of its machining, frequent replacement of this part is impractical. At run 43, a switch was made from operation with “half” capacitor bank to operation with the full capacitor bank. Runs 43 – 45, with the full capacitor bank and the spider, were substantially better, on the average, than runs 34 – 42 [“bad” spider configuration (with “half” capacitor bank)], with respect to test times and shock wave tilt time delays, despite the presence of a “double” shock in run 44. A decision was made to stay with the spider configuration and full capacitor bank for subsequent entries.

IIIB. ENTRY 53B

After the initial 45 runs of Entry 53, the tube was dismantled and weld welts hand machined to improve the interior contour of the tube. (It was discovered to be impossible to bore a circular cross-section down the tube due to non-uniformity in its construction). As discussed above, this machining did not eliminate the welts due to concerns about the tube wall becoming too thin. Nevertheless, the tube was reassembled over a year later and tested again for performance. This was considered a continuation of the previous Entry 53 and thus known as Entry 53B. Figure 10 shows the seven tube configurations investigated in this test entry. These configurations are listed below. The 30 inch long driver is cylindrical and is shown in Fig. 11.

Configuration (a), runs 1 - 4, 7: conical driver, 10 degree cone
Configuration (b), runs 5, 6: conical driver, no cone
Configuration (c), runs 8 – 13: 30 inch driver, 10 degree cone
Configuration (d), runs 14, 15: 30 inch driver, 10 degree cone with buffer
Configuration (e), runs 16 – 18: 30 inch driver, 15 degree cone
Configuration (f), runs 19, 20: conical driver, 15 degree cone with buffer
Configuration (g), runs 21 – 26: 30 inch driver, 10 degree cone

Note that configuration (g) appears identical to configuration (c). However, the ordering of the 24 in tube sections is different for these 2 cases – this change will be discussed at a later point. Configuration (a) is the same as that used in Entry 53. The spider trigger wire arrangement was used for all runs of Entry 53B, except for the first run, in which the cross-wire trigger wire arrangement was used.

The following parameters were used in Entry 53B.

Driver gas: helium at 100 – 152 psia
Conical driver volume: 1292 cm^3
30 inch driver volume: 6645 cm^3
Capacitor bank voltage: 19 – 27 kV
Diaphragms for conical driver: 0.012 inch thick 1100-O aluminum
Diaphragms for 30 inch driver: 0.063 inch thick 304 stainless steel with 30% deep grooves
Driven gas: ~0.05 Torr Mars gas (96% CO_2/4% N_2) except for run 7, which was 0.10 Torr Mars gas

Note that the volume of the 30 inch driver is about 5 times greater than that of the conical driver and also that the 30 inch driver requires (based on past history) much thicker diaphragms than the conical driver. Capacitor bank voltages are somewhat lower for Entry 53B than for Entry 53 because Entry 53B used the full capacitor bank, whereas Entry 53 (with the exception of the last 3 runs) used “half” capacitor bank.

Various plots of the data for Entry 53B are shown in Figs. 12 - 19. Figure 12 shows the test time (free of driver gas contamination) versus run number. Figure 13 shows the shock wave tilt time delay at station K versus run number. Figure 14 shows the half-widths of the spectrometer light peaks versus run number. The half-width is defined as the full width of the light peak at half the full amplitude. Figures 15 – 19 show the shock wave tilt time delays versus distance along the tube for various facility configurations.

From the test times and shock wave tilts shown in Figs. 12 and 13, no advantage was found in removing the 10 degree cone (for runs 5 and 6) as compared to the results with the cone in place (runs 1 – 4 and run 7). Hence, it was decided to keep a cone (either the 10 degree cone or the 15 degree cone) in place for all succeeding tests. For runs 1 – 7 with the conical driver, test times were short for 5 of the 7 runs (Fig. 12). Hence, it was decided the change to the 30 inch driver. The volume of the 30 inch driver is 5.1 times greater than that of the conical driver. Hence, for the same driver gas pressure and capacitor bank voltage, the energy density in the driver gas will be 5.1 times for the 30 inch driver. Thus, it would be expected that driver gas jets driving into the driven gas (test gas) will be weaker for the 30 inch driver and will not penetrate as far into the driven gas, leading to longer contamination free test times. With the 30 inch driver, all four runs for which we have data (runs 10 – 13) showed good test times (see Fig. 12). (Test time data was not obtained for runs 8 and 9 due to camera trigger problems.) Shock wave tilt time delays are better, on the average, with the 30 inch driver than with the conical driver (see Figs. 13, 15 and 16), however, the light curves were unsatisfactory except for the case of run 10. The light (radiance) curves for runs 10 and 11 are shown in Figs. 20 and 21. Run 10 had acceptable light radiance curves while run 11 had unacceptable radiance curves with significant kinks. The radiance curves for runs 12 and 13 (not shown here) were also

unacceptable. The superior light curves for run 10 are also evidenced in the shorter light peak half widths for this run shown in Fig. 14.

For certain operating conditions with the 4 inch driven tube, placing a buffer at an intermediate pressure between the driver and driven tubes had been found to increase the test time. Hence, after the 30 inch driver runs (runs 8 to 13), the buffer configuration of Fig. 6(d) (still with the 30 inch driver) was tried. The buffer was 40 inches long and filled with 20 Torr of helium. Both of these buffer runs had very short test times (see Fig. 12). The shock radiance traces showed fast light rise times, but wide non-equilibrium shock zones with irregular structure in the decay region (Fig. 22), so this buffer configuration was abandoned.

The 10 degree cone discussed thus far was mounted inside of the 24 inch tube. This requires a step transition from the end of the cone to the tube ID. The height of this step was 0.5 inch. It was speculated that this step caused wave patterns to propagate down the tube. Hence, an external cone with a 15 degree angle was manufactured which eliminated the step, and resulted in a continuous diameter increase from 4 inches to 24 inches, but with abrupt changes of angle from zero to 15 degrees to zero at the two ends of the cone. This was used in the configuration of Fig. 6(e). With this configuration, runs 16 and 18 had double shocks and all three runs, especially runs 17 and 18, had large shock tilt time delays. The inferior performance of this configuration regarding shock wave tilt when compared with the 10 degree cone results (runs 8 - 12) can be seen in Figs. 13, 16 and 18. The inferior performance of the 15 degree cone may not be due to the cone itself but, rather, to the fact that with the 10 degree cone, there is a 40 inch run of 4 inch tube between the driver and the cone entrance, whereas, with the 15 degree cone, the driver discharges directly into the cone. With the 10 degree cone configuration, shock wave tilts originating from the driver have a 40 inch run (L/D = 10) to dissipate before entering the cone. With the 15 degree cone, any shock wave tilt produced by the driver discharges directly into the cone. This 15 degree cone configuration was thus abandoned in favor of the next configuration.

A hybrid combination of conical driver, buffer and 15 degree cone was tried next [see Fig. 6 (f)]. The buffer length was 34 inches and helium buffers at 20 and 75 Torr pressure were tried. As contrasted to the previous configuration [Fig. 6(e)], this configuration permits the 15 degree cone to be used with a 34 inch (buffer) calm down length between the driver and the cone. Run 20, with a 75 Torr buffer, had a very short test time (see Fig. 12) and run 19, with a 20 Torr buffer, had significant kinks in the light curves. Both buffer configurations may have suffered because the buffer diaphragm opens directly into the cone, such that any flow non-uniformity produced by asymmetric buffer diaphragm breakage would not have an opportunity to settle down before expanding into the larger tube. Thus, better performance may be realized if the buffer configurations were followed with some run length of 4 inch tubing. This is not possible in the current configuration of the 24 inch tube. It should be noted that the buffer diaphragm is very light (0.001 inch aluminum) and thus, should open almost instantly upon shock arrival and thus, the non-uniformity of buffer diaphragm breakage may be minimal.

Since the buffer configurations and the 15 degree cone configuration of Fig. 6(e) were not successful, it was decided to return to the configuration of Fig. 6(c) with the 30 inch driver, which produced long test times, and attempt to reduce the shock wave tilts and distortions by re-arranging the 24 inch tube sections. As discussed above, there are two obvious reasons for the shock waves to be tilted/distorted: one is the sideways kicks given to the shock waves by the driver due to asymmetries in the arc discharge and diaphragm rupture, the second is the welts in the wall of the 24 inch tube, which were produced when the diagnostic ports were welded in place.

The 24 inch tube is made up of three 20.6 foot long tube lengths plus a test section 3.5 feet long (see Fig. 3). In the tube configuration used up to the present time, the most upstream of the tube lengths has no ports and thus, no weld welts, whereas the two tube lengths further downstream have many ports each and corresponding weld welts. The 3.5 foot long test section is of higher quality than the 20.6 foot long tube lengths and appears to be free of weld welts although it contains diagnostic ports and window ports. For runs 21 – 26, we have the

configuration of Fig. 6(g), which appears to be identical to that of Fig. 6(c), but the 24 inch tube length without ports (and without weld welts) has been moved to be immediately upstream of the test section. Figure 23 shows the arrangement of the diagnostic ports for the configuration of Fig. 6(g) and corresponds to Fig. 3 for the configuration of Fig. 6(c). The configuration of Fig. 6(g) and Fig. 23 gives a 24.2 foot run of smooth tube downstream of the last diagnostic port of the second tube length for the shock wave tilts to calm down before arriving at the spectrometer station. In the original configuration of the 24 inch tube sections, this "calm down" run was only 3.5 feet.

In Fig. 12, we can see that the test times for runs 21 – 26, after the re-arrangement of the 24" tubes, are the same or better as the test times for runs 10 – 13, before the tube re-arrangement. Note that all of runs 21 - 26 had long test times. In Fig. 13, we see that the shock wave tilt time delays at station K for runs 21 – 26 after the tube re-arrangement are all smaller than 3 out of 5 of the time delays for runs 8 – 12 before the tube re-arrangement. The same trend can be seen in Figs. 16 and 19. In addition, none of the spectrometer light curves for runs 21 – 26 had double or triple shocks or kinks. In contrast, for runs 1 – 20, where we had light curves for 16 out of 20 runs, 13 out of 16 of the light curves had unacceptable features and two more of the 16 had short test times, leaving only one out of 20 runs of acceptable all around quality. In contrast, by the same standards, all six of runs 21 – 26 were of acceptable all around quality.

The success rate of runs to this point is measured in terms of light rise time measured on the spectrometer. The cumulative distribution of rise times, or percentage of runs with a rise time less than t, is shown in Fig. 24 for three grouping of runs. First, runs 20 to 45 from Entry 53, which employed a telecentric optics configuration, were analyzed. Only one of these 21 runs had a rise time less than 1 μs. Five of these, or 24%, had a borderline rise times of 1.0 to 1.5 μs. After the tube walls were machined down for Entry 53B, 14 runs using configuration a to c and e and f were analyzed. (Configuration d was omitted due to irregular post-shock structure.) Two of these runs showed rise times less than 1 μs and seven (54%) had rise times between 1.0 and 1.5 μs. In contrast, with configuration (g) 5 out of 6 runs had rise times under 1.0 μs and all runs had rise times under 1.5 μs. This trend provides substantive evidence that the weld welts, which were progressively improved between these three groupings of runs, are a major contributor to shock non-uniformity.

IIIC. ENTRY 59

Following successful demonstration in CO_2-based mixtures, the tube was tested for air mixtures in Entry 59. The shock tube configuration for Entry 59 was that shown in Fig. 6(g), with the 30 inch driver, 10 degree cone and with the 24 inch tubes re-arranged to place the smooth section without ports immediately upstream of the test section. The following parameters were used in Entry 53.

Driver gas: helium at 119 – 123 psia
Driver volume: 6645 cm^3
Capacitor bank voltage:
  14.5 – 19.5 kV for 0.01 Torr driven gas
  21.7 – 27 kV for 0.05 Torr driven gas
  28 – 34 kV for 0.14 Torr driven gas
Diaphragms: various 304 stainless steel, see Table 1 below
Driven gas: 0.01, 0.05 and 0.14 Torr air

Table 1 gives more details regarding the facility operating conditions and diaphragms used. (Note that this table is not strictly in run order but, rather, is organized by driven tube pressure.)

Diaphragm performance will be discussed in a later section. In comparison to Entries 53 and 53B, which used Mars gas as the driven gas, for Entry 59, air is used as the driven gas. Air is 33% less dense than Mars gas at a given pressure. Higher capacitor bank voltages were needed for some runs in Entry 59 than those used in Entry 53B because driven gas load pressures for Entry 59 were up to 0.14 Torr, whereas in Entry 53B, the driven gas load pressures were (with one exception) 0.05 Torr.

Table 1. Facility operating conditions and diaphragms for Entry 59.

Shot #	Driven gas (air) pressure (Torr)	Bank voltage (kV)	Driver gas pressure (psia)	Diaphragm	Diaphragm thickness (in)	Diaphragm groove depth (%)	Estimated diaphragm rupture pressure (psi)	Driver energy pressure (psi)	(Estimated diaphragm rupture pressure)/ (driver energy pressure)
59/1	0.05	21.6	121	30D - Threw tips	0.060	30	2950	4957	0.595
59/2	0.05	27	121	403 - Threw tips	0.090	33.6	4427	7746	0.572
59/3	0.05	26.3	119	404	0.120	37	5740	7349	0.781
59/4	0.05	25.8	119	404	0.120	37	5740	7072	0.812
59/5	0.05	26	121	504	0.120	48	3026	7183	0.421
59/6	0.05	26.3	120	403 - Threw tips	0.090	33.6	4427	7349	0.602
59/7	0.05	26.3	121	304	0.120	26.7	8966	7349	1.220
59/8	0.05	24.5	120	304	0.120	26.7	8966	6378	1.406
59/24	0.05	24.1	122	304	0.120	26.7	8966	6171	1.453
59/25	0.05	23.4	123	304	0.120	26.7	8966	5818	1.541
59/26	0.05	23.9	122	304	0.120	26.7	8966	6069	1.477
59/27	0.05	23.5	122	304	0.120	26.7	8966	5868	1.528
59/28	0.05	23	123	304	0.120	26.7	8966	5621	1.595
59/9	0.01	14.5	120	36D	0.060	36	2200	2234	0.985
59/10	0.01	19.5	121	30D - Threw tips	0.060	30	2950	4040	0.730
59/11	0.01	18.2	121	30D	0.060	30	2950	3519	0.838
59/12	0.01	18.3	120	403	0.090	33.6	4427	3558	1.244
59/13	0.01	18.5	120	403	0.090	33.6	4427	3636	1.217
59/14	0.01	18.9	120	403	0.090	33.6	4427	3795	1.166
59/15	0.01	18.9	120	403	0.090	33.6	4427	3795	1.166
59/29	0.01	18.9	121	403	0.090	33.6	4427	3795	1.166
59/30	0.01	18.9	123	403	0.090	33.6	4427	3795	1.166
59/31	0.01	18.9	121	403	0.090	33.6	4427	3795	1.166
59/32	0.01	18.9	123	403	0.090	33.6	4427	3795	1.166
59/33	0.01	18.9	122	403	0.090	33.6	4427	3795	1.166
59/16	0.14	35	120	PN6 (506)	0.185	48	5847	13016	0.449
59/17	0.14	30.7	120	PN6 (506)	0.185	48	5847	10014	0.584
59/18	0.14	29.9	121	304	0.120	26.7	8966	9499	0.944
59/19	0.14	28.3	121	304	0.120	26.7	8966	8509	1.054
59/20	0.14	28	122	304	0.120	26.7	8966	8330	1.076
59/21	0.14	28.1	122	304	0.120	26.7	8966	8390	1.069
59/22	0.14	28.3	122	304	0.120	26.7	8966	8509	1.054
59/23	0.14	28.3	122	304	0.120	26.7	8966	8509	1.054

- good shot
- doubtful shot
- shot missing spectra
- bad shot

Various plots of the data for Entry 59 are shown in Figs. 25 - 30. Figure 25 shows the test time (free of driver gas contamination) versus run number. Figure 26 shows the shock wave tilt time delay at station K versus run number. Figure 27 shows the half-widths of the spectrometer light peaks versus run number. Figures 28 – 30 show the shock wave tilt time delays versus distance along the tube for the three driven tube gas pressures.

For the test time discussion (see Fig. 25), we divide the test times into “short” test times, 0 – 8 μs long, and “long” test times, greater than 8 μs long. “Long” test times are needed to allow the light emission to relax to equilibrium levels, especially for the lower driven tube pressures. For the 0.14 Torr driven tube pressure runs, there were 6 out of 7 runs (86%) with long test times. For the 0.05 Torr driven tube pressure runs, there were 8 out of 13 runs (62%) with long test times. Finally, for the 0.01 Torr driven tube pressure runs, there were 6 out of 10 runs (60%) with long test times. For the lowest pressure series of runs, two of the runs had zero test time. For the two higher pressure series of runs, none of the runs had zero test time. It is believed that the higher driven tube pressures are more effective at holding back the driver gas jets, which are the main cause of contamination of the driven tube test gas.

The shock wave tilt time delays (see Fig. 26) are considered to be “small” if they are less than 1.3 μs and “large” otherwise. At a typical shock velocity of ~7 km/s, this time delay translates to shock wave tilt angle of ~0.86 degree and axial difference in shock wave location of ~0.9 cm across the 24 inch diameter tube. For the two higher driven tube pressures, the shock wave tilt time delays were small in most cases, being large for only one run at 0.14 Torr driven tube pressure and two runs at 0.05 Torr driven tube pressure. In contrast, at 0.01 Torr driven tube pressure, all except one of the shock wave tilt time delays were large. It is believed that the higher driven tube pressures are less affected by non-uniform driver diaphragm ruptures produced by asymmetric arc strikes. That is, a given sideways kick from the driver will set the driven tube gas into less of a rocking motion at higher driven tube gas densities (and pressures). Additionally, disturbances from the upstream weld welts may not dissipate effectively at lower driven gas loadings, even with the long run length afforded by the tube re-arrangement. The large effect of the driven tube pressure on the shock wave tilt time delays is clearly shown in Figs. 28 to 30, which show the time delays plotted versus distance along the tube.

Figure 27 shows the half-widths of the spectrometer light peaks versus run number. Also shown across the bottom of the figure are the assessments of the quality of the runs (with a key in the top left of the figure). These assessments are made based on test time, shock wave tilt time delays and the shape of the spectrometer light curves. It was found that, in many cases, the half-width of the light peak gives a good indication of whether a run is of acceptable quality. For runs at 0.05 Torr pressure, there is a fairly good correspondence between short light peak half-widths and acceptable quality runs. For the runs with the blue and VUV spectrometers (runs 1 to 8), the runs with the shortest half widths (runs 2, 3, 7 and 8) are exactly the runs judged to be good by the various criteria mentioned above. For the runs with the red and IR spectrometers (runs 24 to 28), the runs with the shortest half widths (runs 24, 25 and 27) are, in two out of three cases, the runs judged to be good. The exception is run 25, with a short half-width, but with an early kink in the red trace, indicating a double shock.

For runs at 0.14 Torr pressure, there is a good correspondence between short light peak half-widths and acceptable quality runs for runs 16 – 20, with the blue and VUV spectrometers. For the runs with the red and IR spectrometers (runs 21 to 23), all judged to be good, the half-widths are larger than the half-widths of runs 16 and 20, judged to be good and are roughly of the order of the half-widths for runs 17 and 18, judged to be bad. However, for the runs at 0.05 Torr pressure, the good runs with the red and IR spectrometers have half-widths somewhat larger, on the average, than those for the good runs with the blue and VUV spectrometers, so the somewhat larger half-widths of the good runs at 0.14 Torr for the red and IR spectrometers may not be inconsistent with using the half-widths to assess run quality.

For runs at 0.01 Torr pressure, there is limited correspondence between short light peak half-widths and acceptable quality runs. This is because the relaxation is slow enough that the light peaks are broadened naturally, making the light peak half-widths an imprecise metric of facility performance. For the runs with the red and IR spectrometers (runs 30 to 33), the good runs (runs 31 and 32 – note that for run 31, only one spectrogram was obtained) have half-widths about 20% less than those for the bad runs (runs 30 and 33). However, for runs 10 – 15, with the blue and VUV spectrometers, the half-widths for the good runs (runs 12 and 15) are very little different than those for the neighboring bad runs (runs 13 and 14).

Overall, it appears that the half-widths of the light peaks have some usefulness in assessing the quality of the runs, but examining the shape of the traces for kinks and multiple shocks is still necessary. The half-widths of the light traces were, however, found to correspond to the run quality much better than light rise-times, which were used at one point. This is because a number of light traces have good rise-times and light rise shapes, but slow light falls or humps on the light falls. This is illustrated in Fig. 22, which shows the wavelength integrated light emission at the blue spectrometer plotted versus camera pixel number for three runs in entry 53B. All three graphs show satisfactory light rises, but the curves for runs 14 and 15 both show

a hump on the light fall.

The overall success rates (runs assessed to be good divided by total number of runs) were 5 out of 8 (63%) for 0.14 Torr pressure, 6 out of 13 (46%) for 0.05 Torr pressure and 3 out of 12 (25%) for 0.01 Torr pressure. Note that the success rate for 0.05 Torr for Entry 59 is much less than the final success rate for this pressure for Entry 53B (runs 21 – 26). The latter success rate was 100%. This is partly due to the higher density of CO_2 relative to air. As mentioned previously, the higher driven tube gas densities are believed to be more effective at holding back the driver gas jets, which are the main cause of contamination of the driven tube test gas.

These low success rates, though better than for the 4 inch tube operation at comparable pressures, are highly undesirable, since they would cause test entries to be substantially extended to obtain the needed number of good test runs. A major cause of failed runs are tilted and/or distorted shock waves, which can manifest themselves as smeared out light peaks, and kinks in the light traces. As discussed in Sec. III, two causes of tilted/distorted shock waves are the weld welts in the wall of the 24 inch tube and sideways kicks produced by asymmetric j x B forces in the driver. To deal with the first issue, it is proposed to fabricate a new set of 24 inch tubes, with a much higher inner surface quality than that of the existing tubes. The second issue cannot be eliminated, but by adding an 8 foot length of 4 inch tube just upstream of the cone in the configuration of Fig. 6(g), additional distance for the shock waves tilts produced by the driver to calm down can be provided. Note that 8 feet of 4 inch tube provides an L/D of 24 for the shock wave to calm down, which is equivalent to 48 feet of 24 inch tube. For comparison, the existing three 20.6 foot long 24 inch tube sections provide a total L/D of 30.9. The increased frictional velocity loss caused by inserting the eight foot length of 4 inch tube is estimated to be 0.7 km/s, which is deemed acceptable. (The driver would have be operated at a slightly higher energy level to achieve a given shock velocity when the eight foot length of 4 inch tube is used.)

IV. DIAPHRAGM DISCUSSION

One of the issues with flat scored diaphragms is the loss of petal tips or whole petals. These can be thrown down the tube at substantial velocities. In a different shock tube facility at NASA Ames (with a 17 inch driver and a 12 inch driven tube), it was observed that, during one particular shot, petals were thrown down the tube at velocities of ~1 km/s, causing major damage to the facility. Clearly, it would be desirable to avoid the throwing of petal tips and, especially, whole diaphragm petals down the driven tube. Figure 31 shows ruptured diaphragms from entries 53B and 59. Fig. 31(a) show a diaphragm with whole petals thrown, Fig. 31(b) shows a diaphragm with petal tips thrown and Fig. 31(c) shows a good diaphragm break. When a whole petal is thrown, it is a triangle 3 – 4 inches wide at the base and 1.5 – 2 inches high. Petal tips are typically triangles roughly 1 inch wide at the base and roughly 0.5 inches high. The diaphragms used in Entry 59 are shown in Table 1. In the present discussion, diaphragm data from Entries 53B and 4B will also be used. (Entry 4B was performed in the 1968 – 1971 time frame.) Figure 32 shows a plot of capacitor bank energies versus diaphragm thickness for the three EAST entries. Symbols for the different entries are in different colors. The different types of symbols, crosses, circles and squares, indicate no diaphragm material lost, petal tips thrown and whole petals thrown, respectively. The various regions of petal material lost are separated by lines. All data is for the 30 inch driver, but it is noted that for the old entry 4B, most of the driver fill pressures were 272 – 441 psi, whereas for entries 53B and 59, the driver fill pressures were ~120 psi.

It would seem highly desirable to avoid the region where whole diaphragm petals are thrown. Ideally, to avoid any risk of damage to the facility (especially to the diagnostic windows and pressure transducers), it would be desirable to operate in the region where no diaphragm material is lost. However, this may sometimes limit the attainable shock velocities below those needed to match the space flight conditions which it is desired to simulate. It may, then, be appropriate to accept some risk and operate in the zone where “petals tips are sometimes

thrown", especially if the thrown petal tips are small, as was occasionally noted in the log books. In the "petal tips sometimes thrown" region for the 0.060 inch thick diaphragms, tips were thrown ~16% of the time. In the "petal tips sometimes thrown" region for the 0.180 inch thick diaphragms, tips were thrown ~35% of the time.

Figure 33 shows the measured rupture pressures (red data points and curve fit) for 0.060 inch thick 304 stainless steel EAST diaphragms. These rupture pressures were obtained by slowly (over a period of several minutes) increasing the gas pressure behind the diaphragm. The blue curve shows corresponding predicted rupture pressures using Eq. (1) of Ref. 10 with the value of $Ar^{0.5}$ = 94,500 bar x $mm^{0.5}$ given in the reference. A is equal to $\sigma_{el}/(1 + \nu)$ where σ_{el} and ν are the elastic limit and Poisson's ratio, respectively, for the diaphragm material. r is the radius at the bottom of the diaphragm grooves. It is seen that the agreement between prediction and experiment is reasonably good for score depths of 43 to 50% but becomes substantially worse as the score depth decreases from 43 to 30%. Reference 10 (Fig. 1 of the reference) presents three sets of comparisons between predictions using their equation and experimental results. Good agreement is noted. However, Ref. 10 also cautions that these comparisons are based upon limited experimental results and do not take account of the rate of pressure rise. Also, note that the experimental results of Ref. 10 are for rapid pressure rises (i.e., diaphragms facing a chamber in which gunpowder was burnt) whereas the EAST diaphragm rupture pressures were obtained quasi-statically.

With the preceding paragraph as background, the following procedure was used to estimate diaphragm rupture pressures for the EAST facility. For 0.060 inch thick diaphragms with score depths between 30 and 50%, the rupture pressures were read directly off the red curve of Fig. 33. For other diaphragm thicknesses, but with score depths between 30 and 50%, the rupture pressures are first read off the red curve of Fig. 33, and then corrected by a diaphragm thickness factor, which is $(\text{thickness ratio})^{1.5}$, taken from section 5 of Ref. 10. Finally, for a 0.120 inch thick diaphragm with a score depths of 26.7%, the blue curve of Ref. 10 was scaled up to match the experimental EAST data at a score depth of 30% (purple curve in Fig. 33), the rupture pressure at a score depth of 26.7% was read off this curve and then the thickness ratio correction of Ref. 10 was applied. These procedures were used to calculate the diaphragm rupture pressures for entry 59 shown in Table 1.

The energy pressure of the driver is estimated assuming that the driver gas (usually helium) follows the ideal gas law. We have, for the pressure

$$p = \rho RT \qquad (1)$$

where

p = pressure
ρ = density
R = gas constant for helium
T = temperature

The gas energy in the driver is given by

$$E = \rho C_v T \times Vol \qquad (2)$$

where

E = gas energy in driver
C_v = specific heat at constant volume
Vol = volume of driver

The specific heat ratio γ, is given by $\gamma = C_p/C_v = (C_v + R)/C_v$, where C_p is the specific heat at constant pressure. Combining Eqs. (1) and (2) with the definition of γ, we get

$$p = (\gamma - 1)E/Vol \qquad (3)$$

Putting the gas energy E equal to the capacitor bank energy, $E_{bank} = 0.5CV^2$, (with bank capacitance = C and bank voltage = V), one obtains the driver energy pressure. This procedure was used to calculate the driver energy pressures for Entry 59 shown in Table 1.

It has been observed that, on the average, better quality runs are obtained when the diaphragm rupture pressures are a greater fraction of the driver energy pressures. For Entry 59, Fig. 34 shows the average values of the ratio (diaphragm rupture pressure)/(driver energy pressure) plotted versus the quality of the runs (bad, borderline and good). As discussed in a number of preceding sections, good quality runs mean smaller shock tilts, better shaped light curves with shorter half-widths of the peaks and longer test times. The data are grouped by the driven tube fill pressures, 0.01, 0.05 and 0.14 Torr.

In Fig. 34, it is noted that a number of normalized rupture pressures are greater than one. This would appear to indicate that the diaphragm should not have ruptured, whereas in fact, the diaphragm did rupture. This is likely due to the uncertainties in the estimates of the diaphragm pressures discussed in earlier paragraphs, for example, the difference between diaphragm behavior under rapid (i.e., shock tube) loading conditions and slow, quasi-static loading diaphragm rupture tests. Nevertheless, Fig. 34 shows a trend, at all three driven tube fill pressures, of improved run quality at increased energy normalized diaphragm rupture pressures. It can be argued that, with the diaphragm opening at a lower pressure, the petals will move more slowly upon opening and the driver gas will spend more time flowing over the petals, which could set up sideways kicks to the flow if the petals do not open exactly symmetrically. On the contrary, with the diaphragm opening at a higher pressure, the petals would get out of the way more quickly and the time to set up sideways kicks would be reduced and hence, the kicks would be less strong.

VI. SUMMARY AND CONCLUSIONS

The NASA Ames East facility was described and the need for testing in the 24 inch tube (as opposed to the 4 inch tube used for most of the testing to date) was given. Entry 53 was discussed. Two arc trigger wire configurations were presented – one with the main (axial) wire connected to a radial wire at the ground end and the other with the main wire connected to a four legged metal spider (like 4 spokes of a wheel) at the ground end. Test times were measured spectroscopically and shock tilts were measured using opposed pairs of pressure transducers. It was concluded that the spider wire configuration was superior and that testing at the higher bank capacitance gave better results. The overall success rate of Entry 53 was approximately 14%. A major factor contributing to this low success rate is believed to be the protrusions (welts) due to welds on the tube wall. The welts are believed to disturb the uniformity of the flow. Therefore the tube was machined to reduce the welts prior to further testing.

Next, Entry 53B was discussed. All but one run were performed with 0.05 Torr Mars gas. Seven different facility configurations were tried. These involved 3 cone configurations – no cone, 15 degree cone and 10 degree cone. (The cone expands from the 4 inch driver to the 24 inch driven tube.) Tests were done with and without a 4 inch diameter buffer between the driver and the cone. Tests were done with the conical driver and with a 30 inch long cylindrical driver. Finally, tests were done with the smooth 20.6 foot long 24 inch driven tube section (without diagnostic ports and, hence, without welts due to welds) at the upstream end and at the downstream end of the 63 foot long driven tube. Diagnostics included test times, shock tilts and half-widths of the shock light pulses (smaller half-widths indicating better conditions). The

success rate in Entry 53 was about 36% without the tube re-arrangement and 100% with the re-arrangement. It was concluded that the best configuration was the 30 inch cylindrical driver, followed by a 40 inch length of 4 inch tube and the 10 degree cone with the smooth 20.6 foot long driven tube section at the downstream end of the driven tube.

Next, Entry 59 was discussed. The best facility configuration found in Entry 53B was used. Tests were done with air at 0.01, 0.05 and 0.14 Torr. The same diagnostic suite used in Entry 53B was used for Entry 59. Success rates were ~50% for the higher two pressures and ~25% at the lowest pressure. These were deemed undesirably low and two changes were proposed to improve the success rates. One was to fabricate new 24 inch tube sections following improved construction practices so that the welds needed for the diagnostic ports do not create significant welts. A second improvement would be to insert an additional eight foot length of 4 inch tube just upstream of the 10 degree cone. This would provide an additional L/D of 24 to calm down shock wave tilts produced by the driver.

Diaphragm results were discussed. Conditions under which diaphragm petal tips or whole petals were thrown down the driven tube were correlated. Experimental quasi-static diaphragm rupture pressures were compared with a correlation given in a literature reference. Based on these results, estimates of rupture pressures for Entry 59 were made. The driver pressure based on driver energy was calculated and ratioed with the diaphragm rupture pressure. Higher values of this ratio were found to correspond to runs with higher quality data.

ACKNOWLEDGEMENTS

Acknowledgements are due for the excellent work of the Ames EAST facility crew, M. S. McGlaughlin, R. Martinez, J. M. Joyce and A. K. Parish. Support by NASA (Contract NNA15BB15C) to Analytical Mechanics Associates, Inc. is gratefully acknowledged.

REFERENCES

1. Grinstead, J. H., Wilder, M. C., Reda, D. C., Cornelison, C. J., Cruden, B. A., and Bogdanoff, D. W., "Shock Tube and Ballistic Range Facilities at NASA Ames Research Center," RTO-EN-AVT-186, 2010.
2. Grinstead, J. H., Wilder, M. C., Reda, D. C., Cruden, B. A., and Bogdanoff, D. W., "Advanced Spectroscopic and Thermal Imaging Instrumentation for Shock Tube and Ballistic Range Facilities," RTO-EN-AVT-186, 2010.
3. Cruden , B. A., "Absolute Radiation Measurements in Earth and Mars Entry Conditions," RTO-EN-AVT-218, 2014.
4. Cruden, B. A., Martinez, R., Grinstead, J. H., and Olejniczak, J., "Simultaneous Vacuum Ultraviolet through Near IR Absolute Radiation Measurement with Spatiotemporal Resolution in an Electric Arc Shock Tube," AIAA Paper 2009-4240.
5. Grinstead, J. H., Wilder, M. C., Olejniczak, J., Bogdanoff, D. W., Allen, G. A., Dang, K., and Forrest, M. J., "Shock-heated Air Radiation Measurements at Lunar Return Conditions," *46th AIAA Aerospace Sciences Meeting*. AIAA, Reno, Nevada, 2008, AIAA 2008-1244.
6. Cruden, B. A., "Radiance Measurement for Low Density Mars Entry," AIAA Paper 2012-2742.
7. Cruden, B. A., Prabhu, D., and Martinez, R., "Absolute Radiation Measurement in Venus and Mars Entry Conditions," *Journal of Spacecraft and Rockets,* Vol. 49, No. 6, 2012, pp. 1069-1079.
8. Grinstead, J. H., Wright, M. J., Bogdanoff, D. W., and Allen, G. A., "Shock Radiation Measurements for Mars Aerocapture Radiative Heating Analysis," *Journal of Thermophysics and Heat Transfer,* Vol. 23, No. 2, 2009, pp. 249-255.

9. Mirels, H., "Test Time in Low-Pressure Shock Tubes," *Physics of Fluids,* Vol. 6, No. 9, 1963, p. 1201.
10. Bernier, H., “Flat Scored High Pressure Diaphragms as Quick Opening Valves,” (in French) presented at the 42nd Aeroballistic Range Association Meeting, October 22 – 25, 1991, Adelaide, Australia.

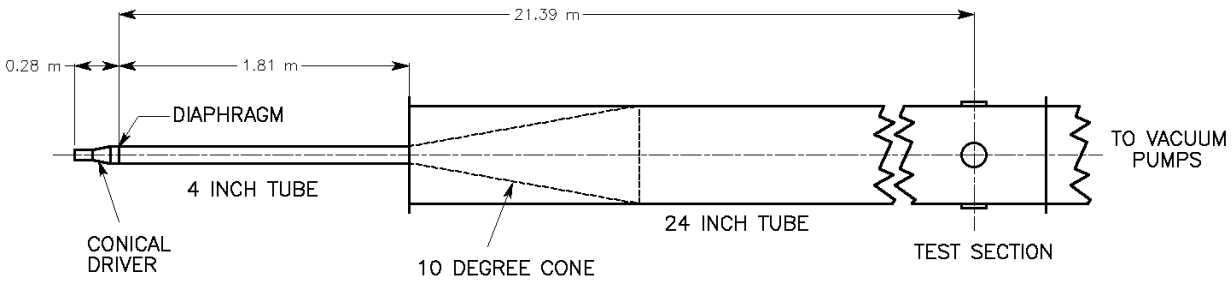

Figure 1. Schematic sketch of EAST 24 inch tube configuration at the beginning of Entry 53.

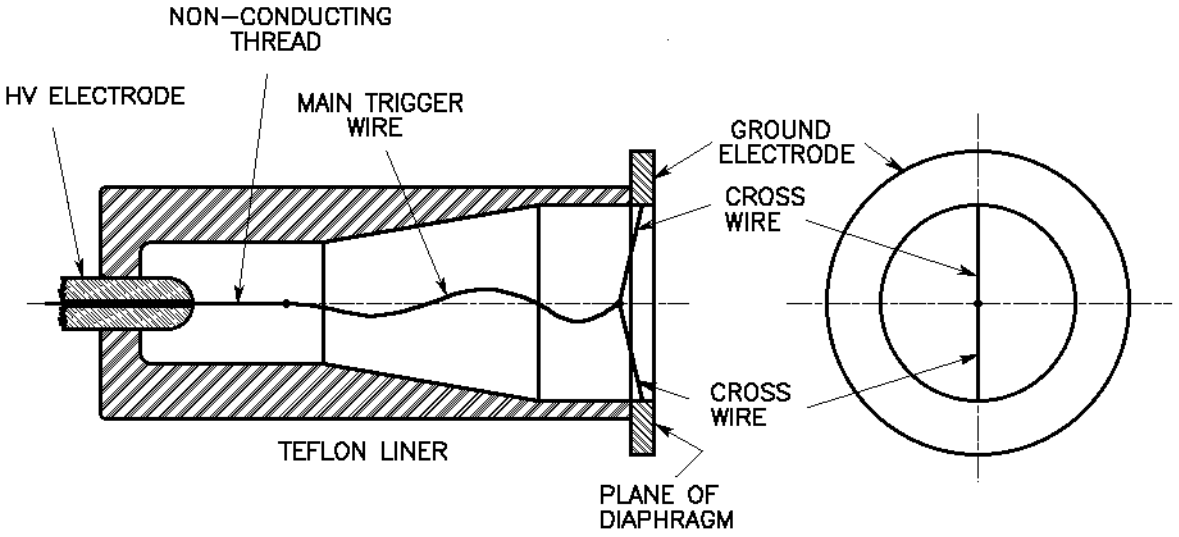

(a) CROSS WIRE TRIGGER WIRE CONFIGURATION

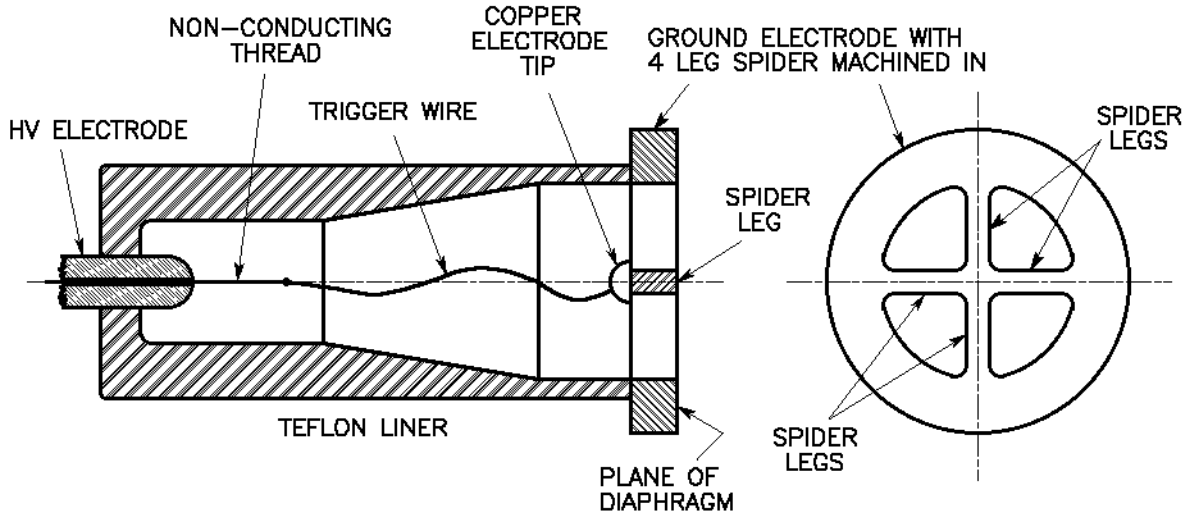

(b) SPIDER TRIGGER WIRE CONFIGURATION

Figure 2. Conical driver arrangements showing two different trigger wire configurations.

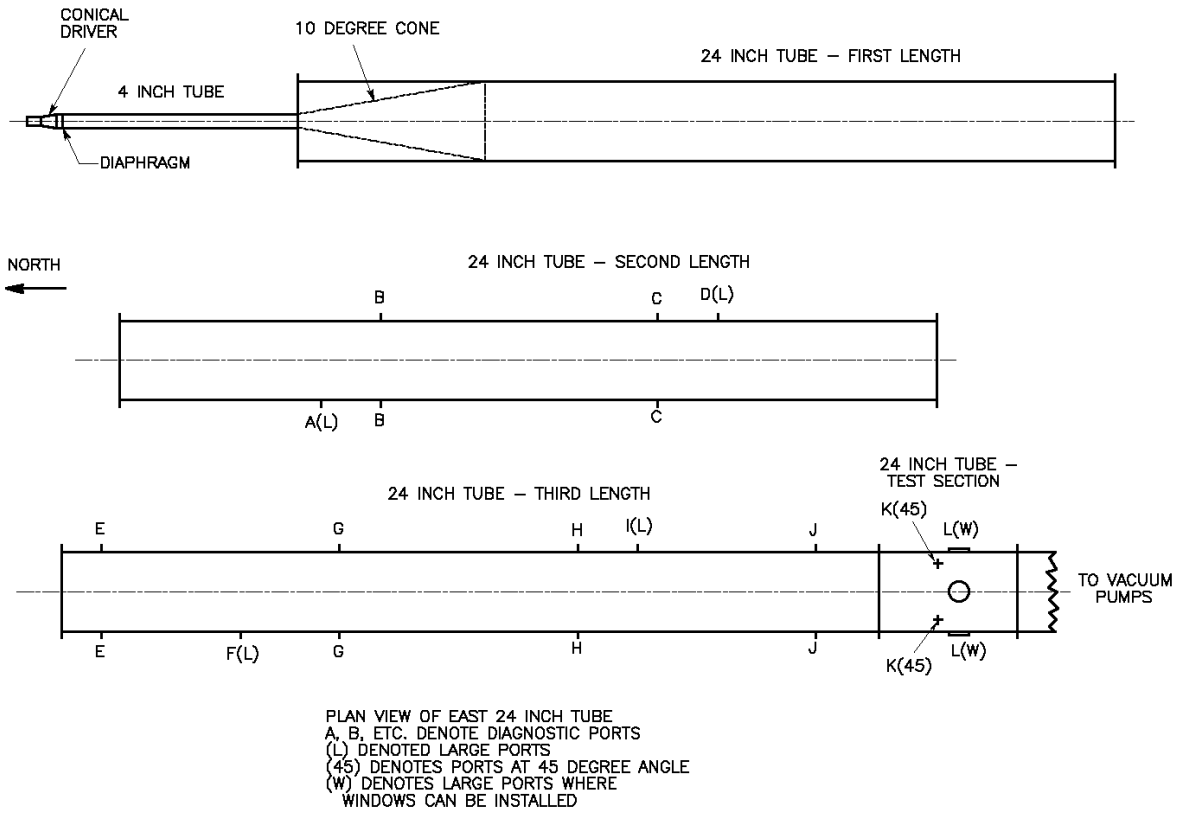

Figure 3. Schematic sketch of EAST 24 inch tube configuration at the beginning of Entry 53. Expanded version of Fig. 1, showing all diagnostic ports.

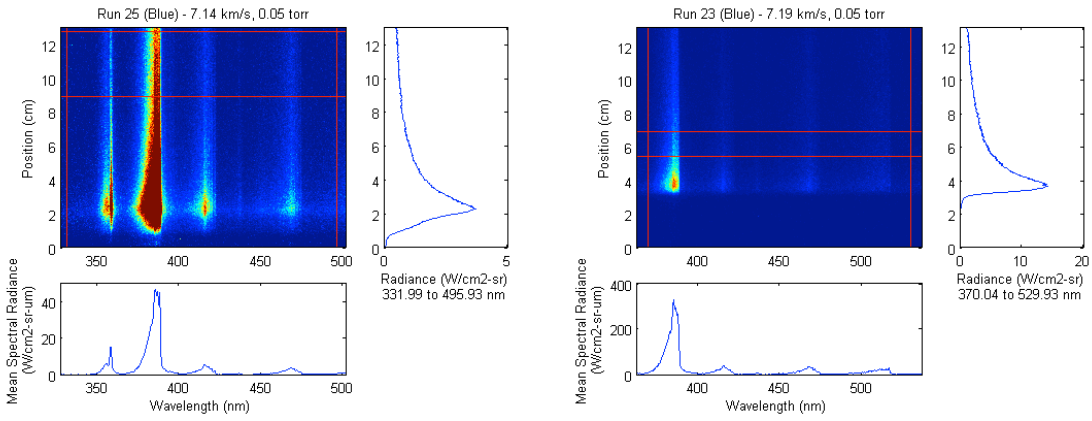

Figure 4. Comparison of "good" and "bad" spectrometer measurements at otherwise similar conditions. The figure on the left came from Entry 53 and shows an intensity rise which is slow and has a slope change. The figure on the right was from Entry 53B after tube rearrangement and is considered to be of good quality, with fast, clean light rise.

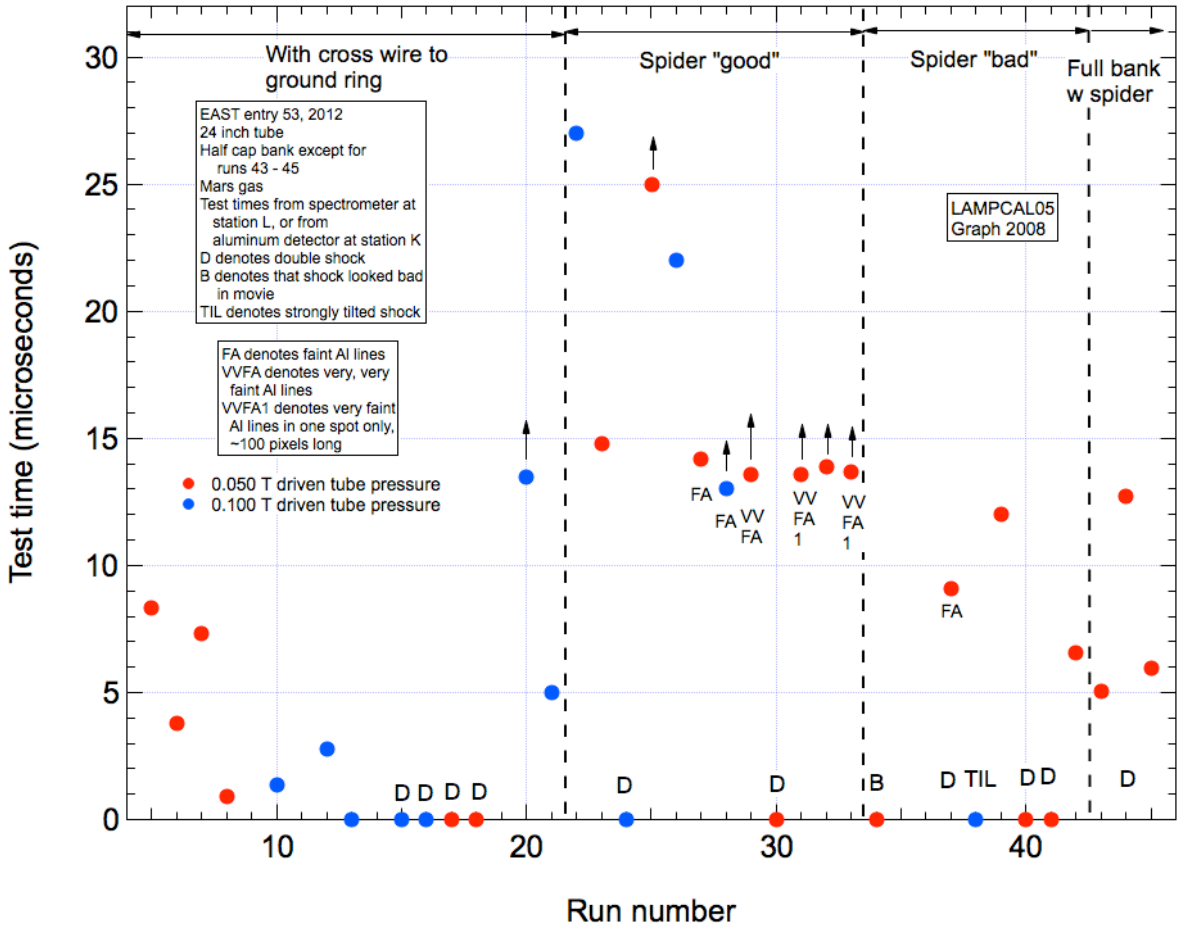

Figure 5. Test time versus run number for Entry 53. Arrows indicate that test times are equal to or exceed those indicated by the data points.

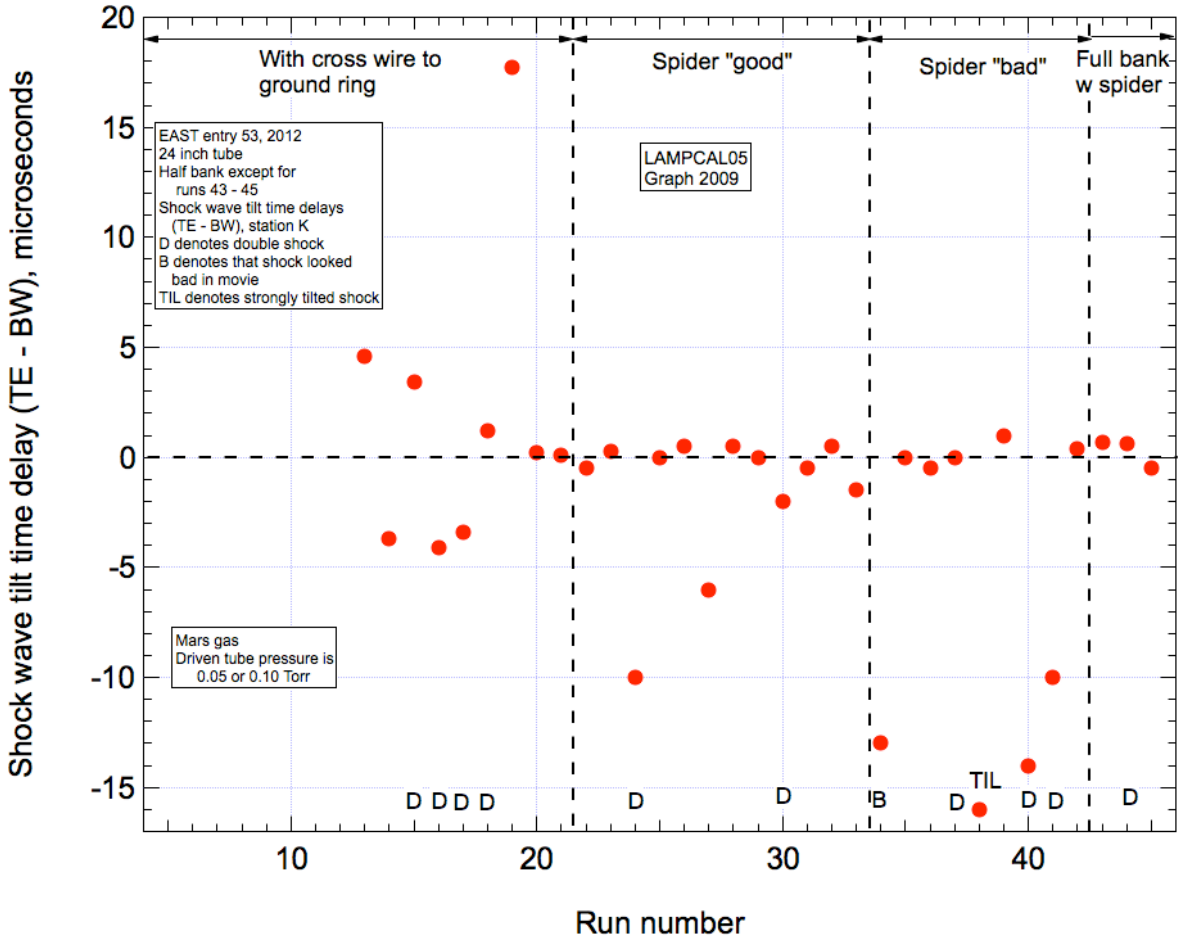

Figure 6. Shock wave tilt time delay versus run number for Entry 53.

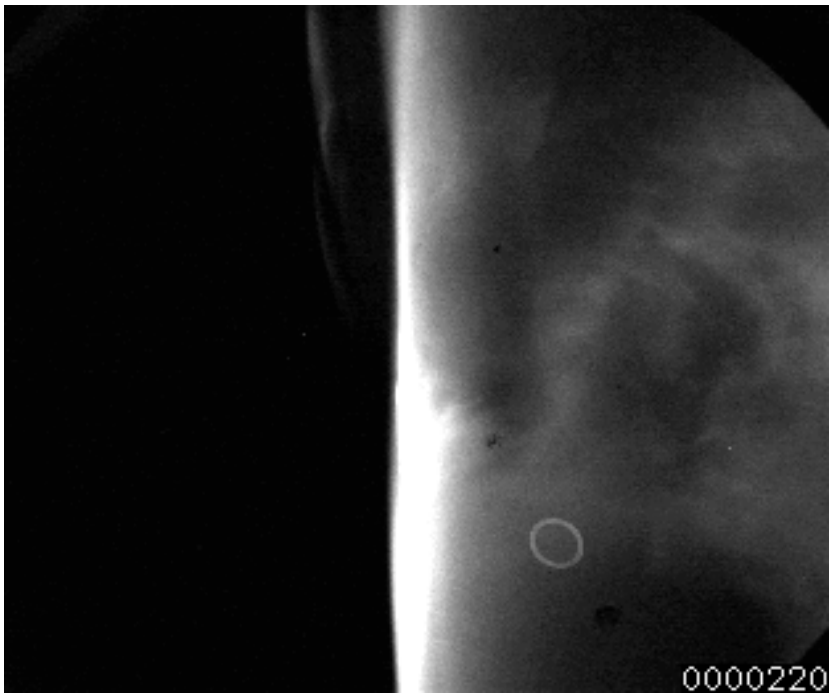

Figure 7. Bottom view of shock wave in test section. Entry 53, run 34. Shock moves towards the left. Height of field of view is 18.5 inches.

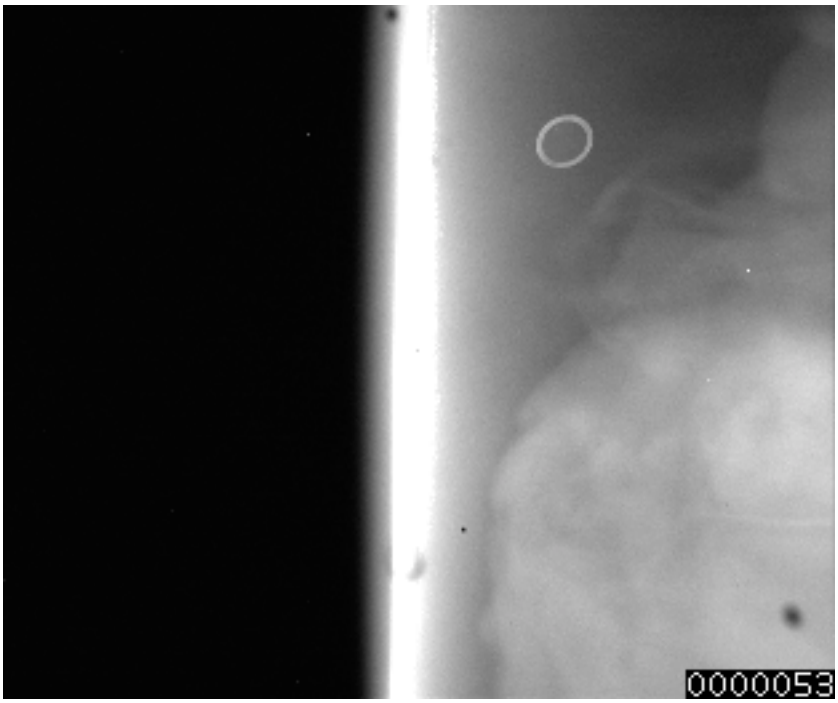

Figure 8. Side view of shock wave in test section. Entry 53, run 35. Shock moves towards the left. Height of field of view is 18.5 inches.

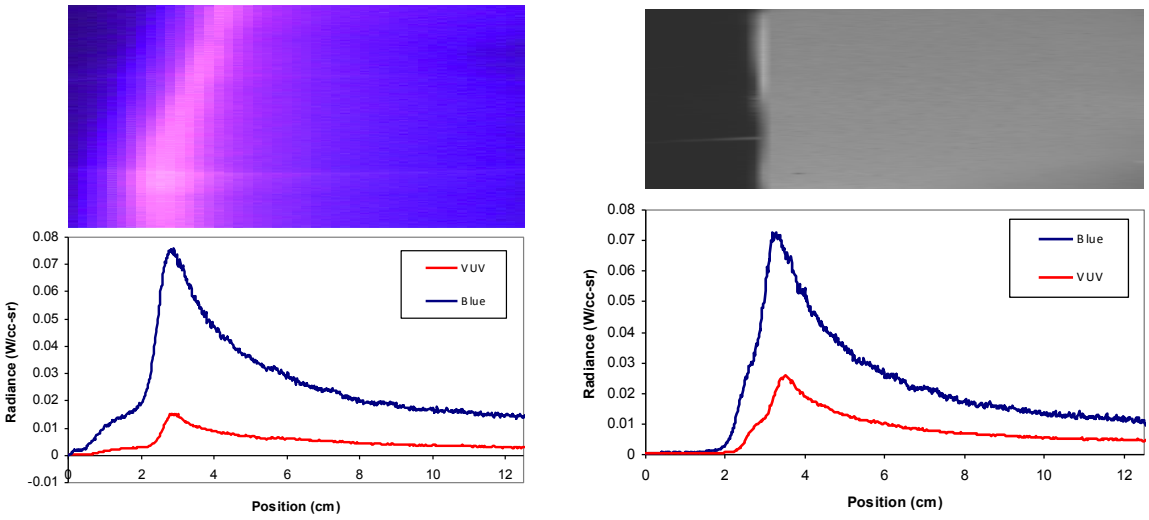

Figure 9. Correspondence of shock images (top) with spectrometer light curves (bottom). Left - Entry 53, run 30 and right - Entry 53, run 36. The shock images have been compressed in the vertical direction relative to the horizontal by a factor of about 12:1.

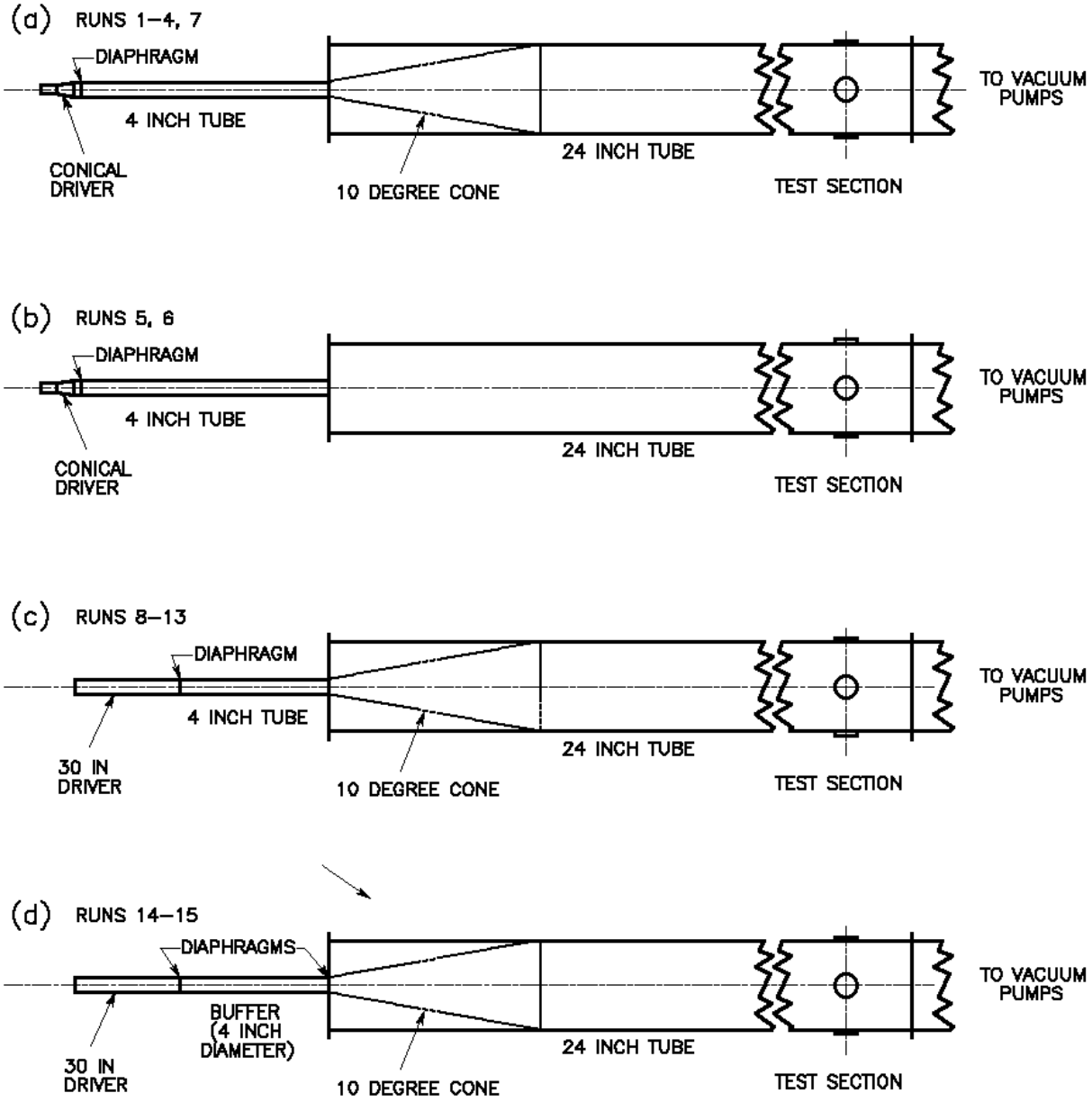

Figure 10. First four shock tube configurations for Entry 53B. (Figure continued on next page.)

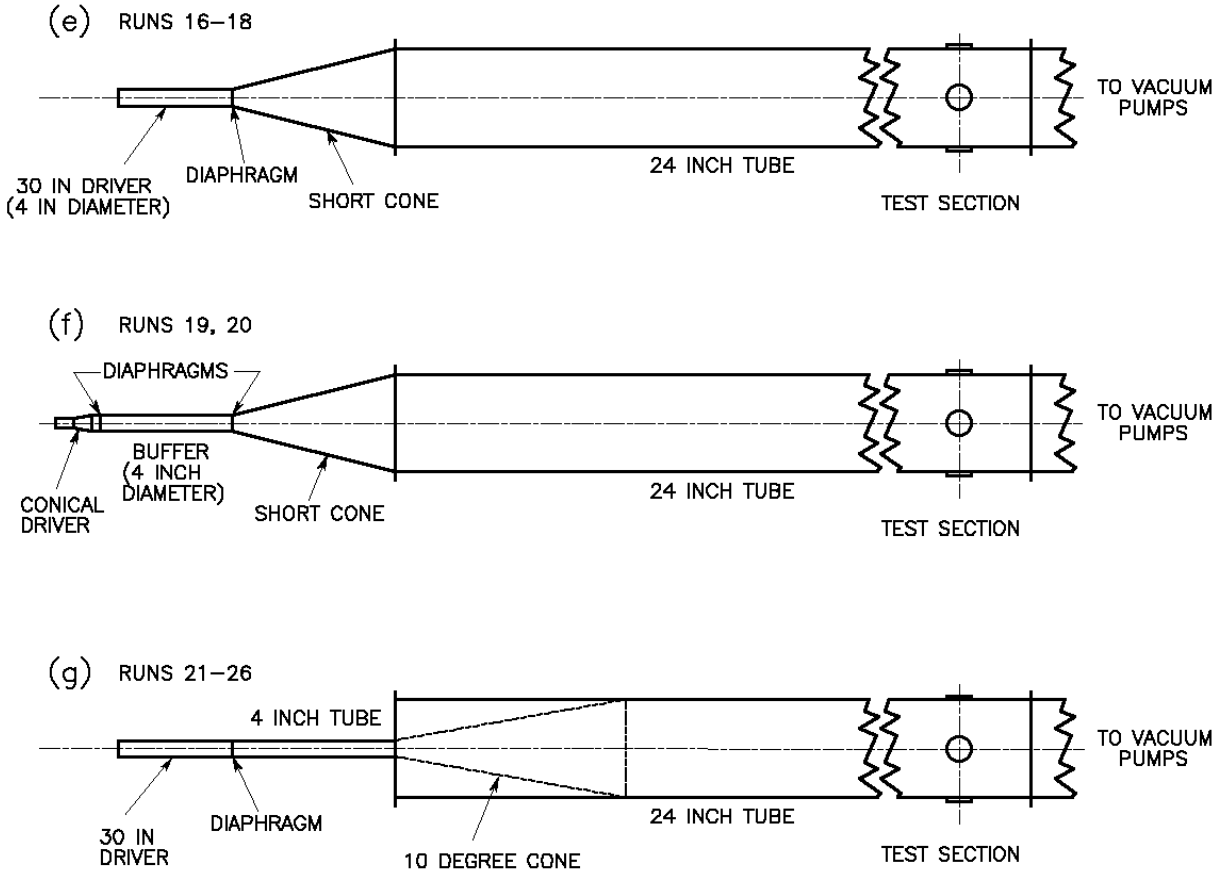

Figure 10 (continued). Final three shock tube configurations for Entry 53B. Note that configuration (g) appears identical to configuration (c). However, the ordering of the 24 in tube sections is different for these 2 cases. See text.

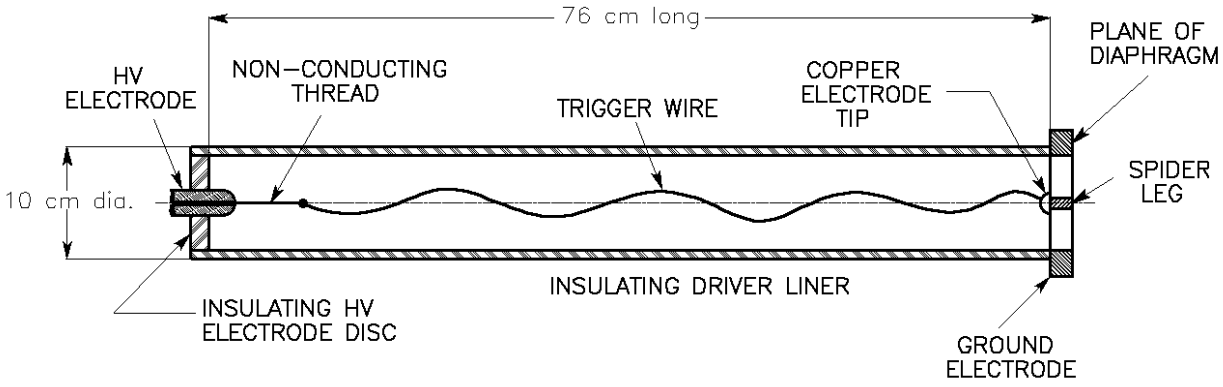

Figure 11. 30 inch driver arrangement.

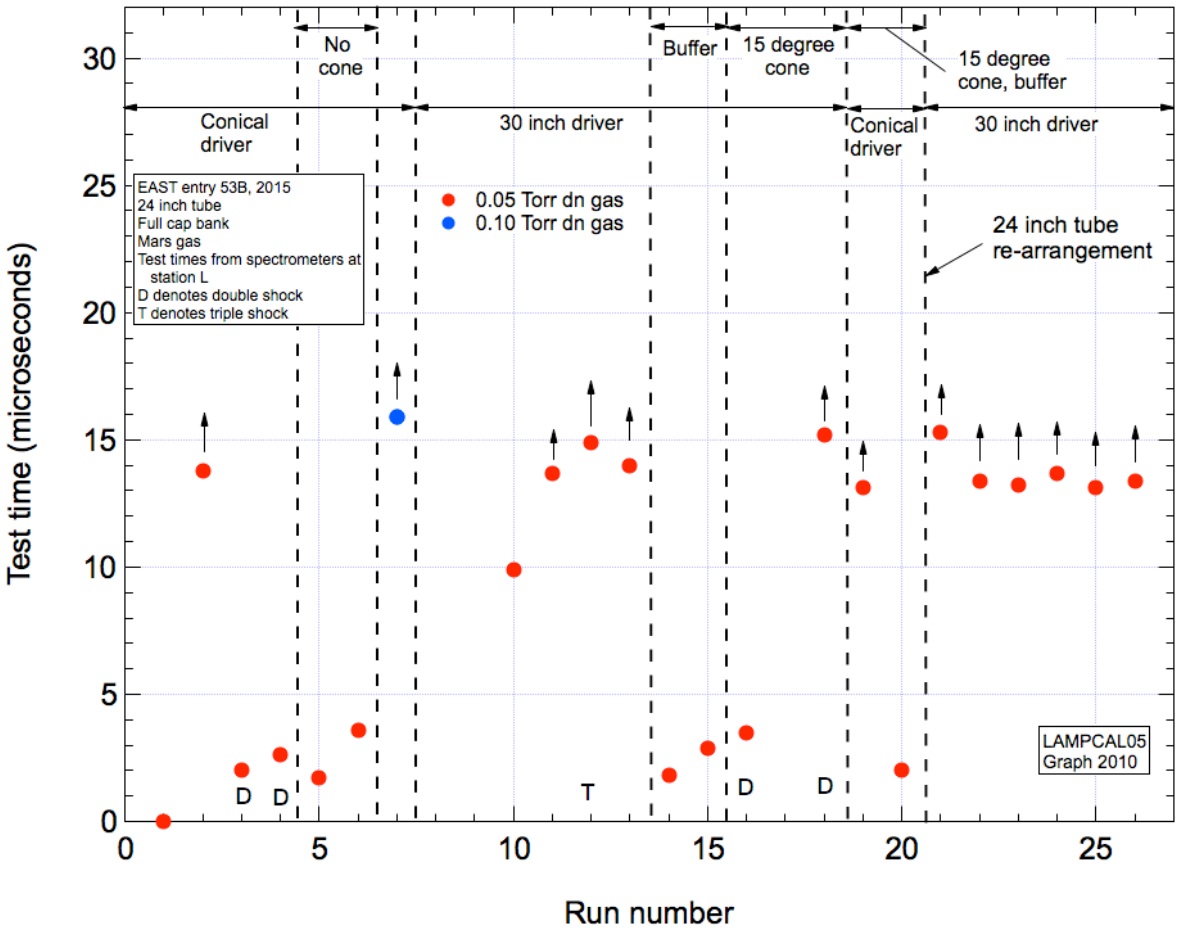

Figure 12. Test time versus run number for Entry 53B. Arrows indicate that test times are equal to or exceed those indicated by the data points.

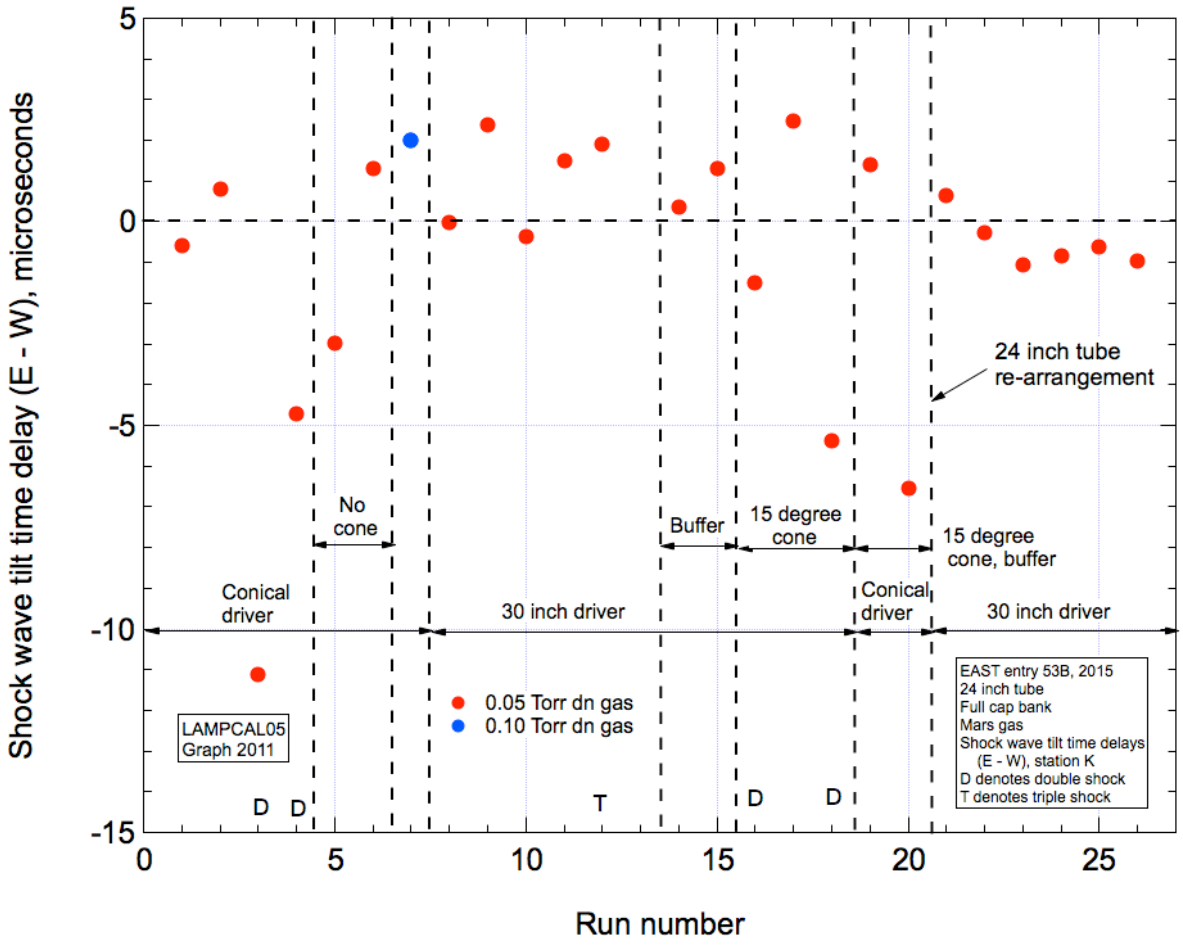

Figure 13. Shock wave tilt time delay versus run number for Entry 53B.

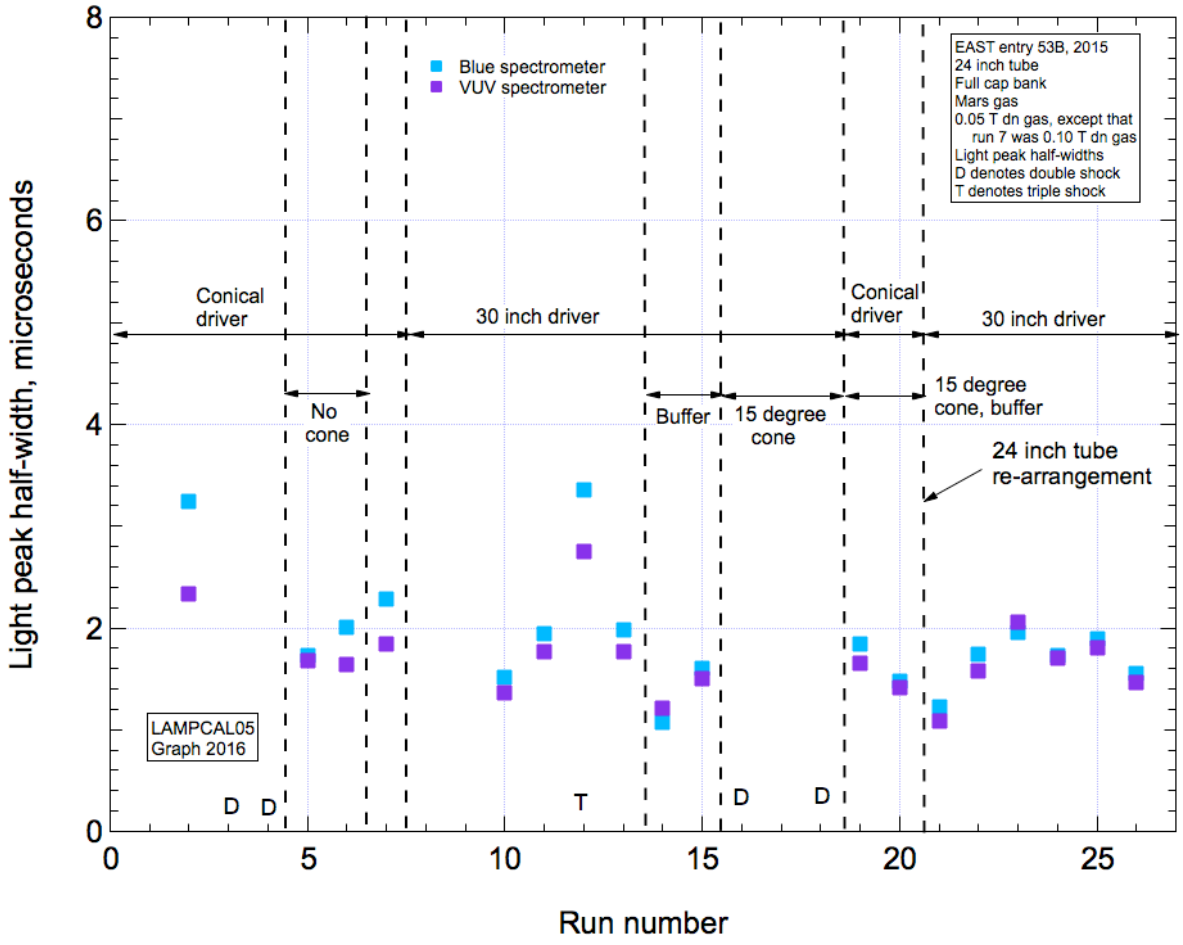

Figure 14. Half-widths of the spectrometer light peaks versus run number for Entry 53B.

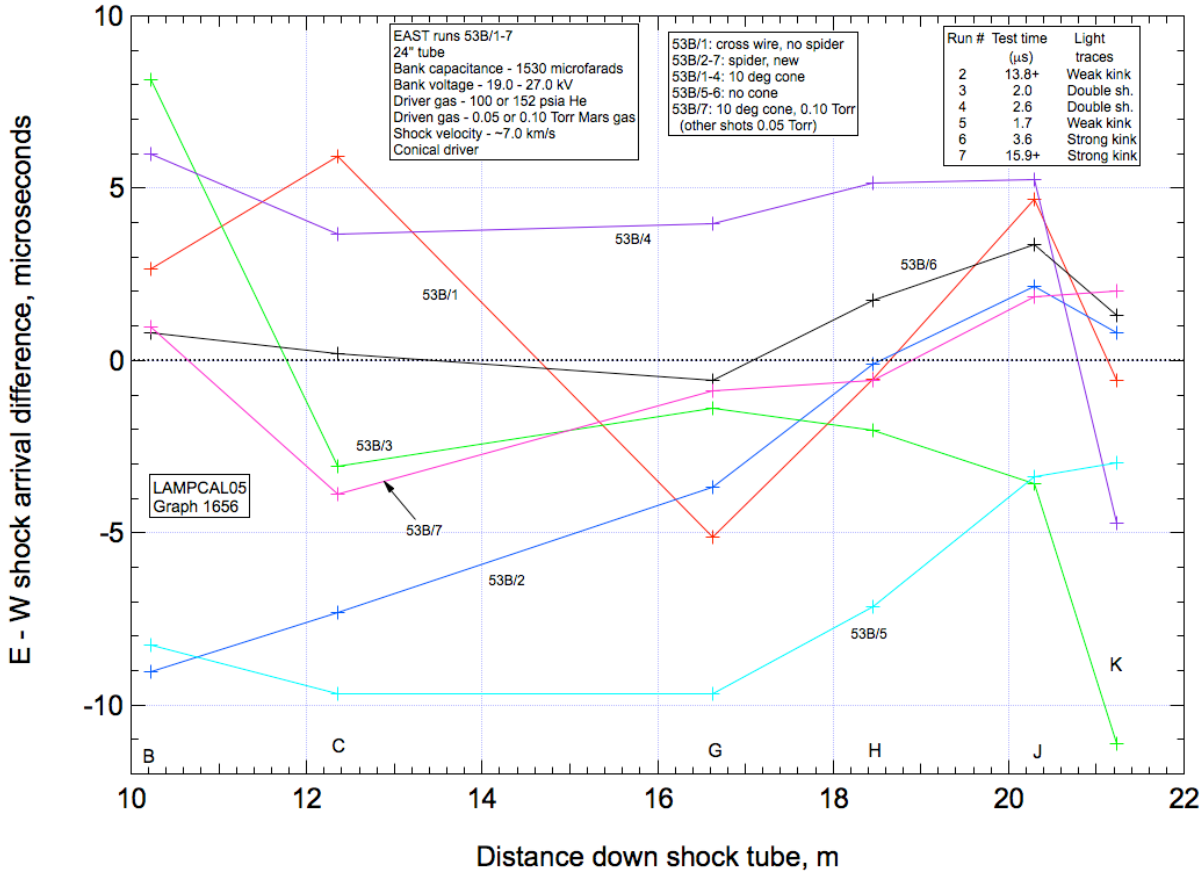

Figure 15. Shock wave tilt time delay versus distance along tube for Entry 53B. This includes data with configurations (a) and (b) which utilized the conical driver with the 10 degree cone or no cone (runs 1 - 7). Letters at bottom refer to diagnostic ports seen in Fig. 3.

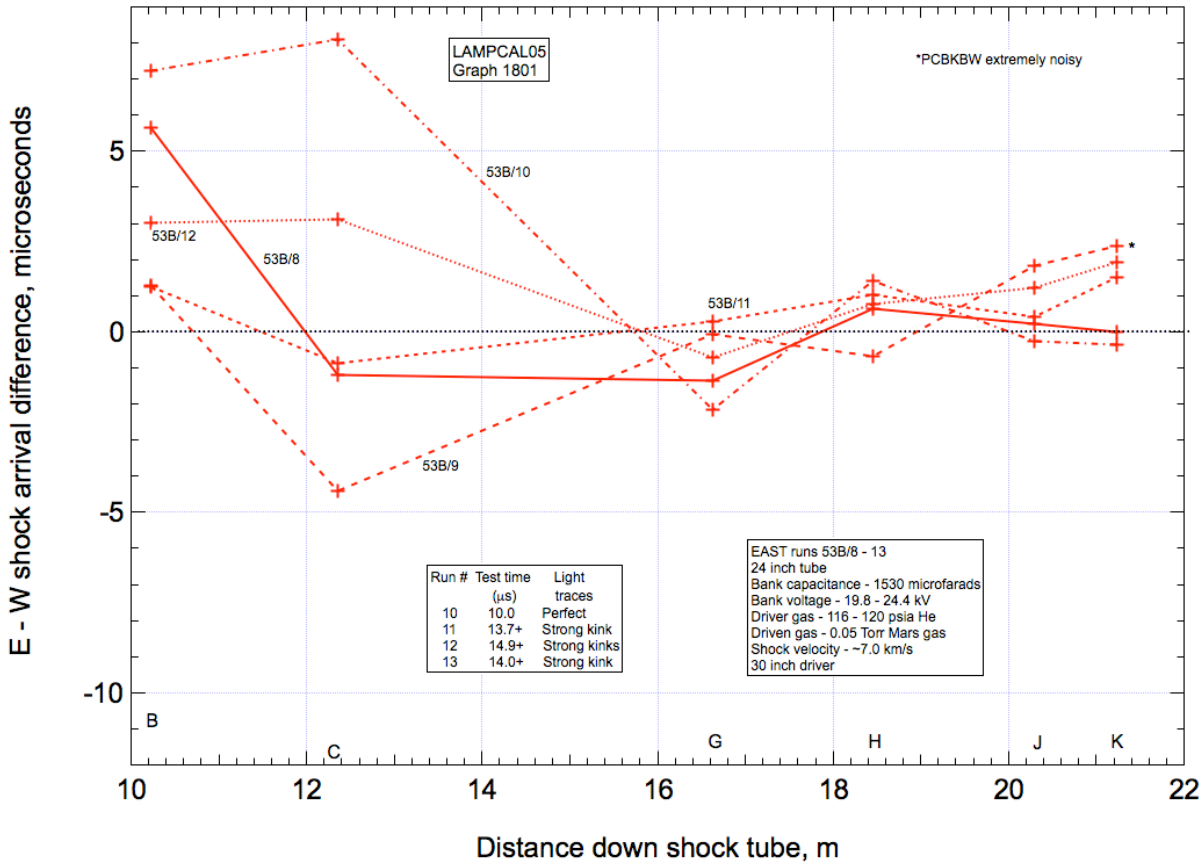

Figure 16. Shock wave tilt time delay versus distance along tube for Entry 53B. These data are from all tests with valid tilt data in configuration (c) – 30 inch driver with 10 degree cone (runs 8 - 12). Letters at bottom refer to diagnostic ports seen in Fig. 3.

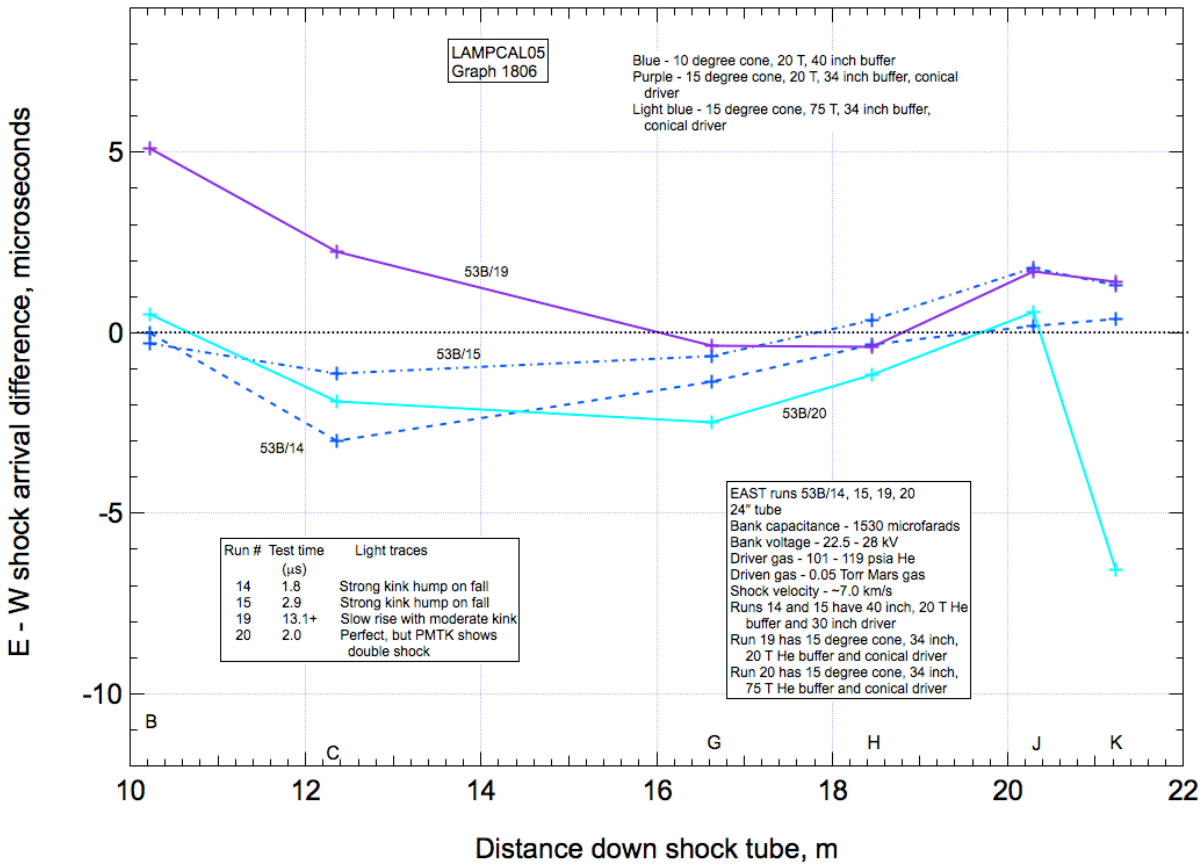

Figure 17. Shock wave tilt time delay versus distance along tube for Entry 53B. This includes data from all buffer tests in configurations (d) and (f), with 10 degree and 15 degree cone, respectively (runs 14, 15, 19 and 20). Letters at bottom refer to diagnostic ports seen In Fig. 3.

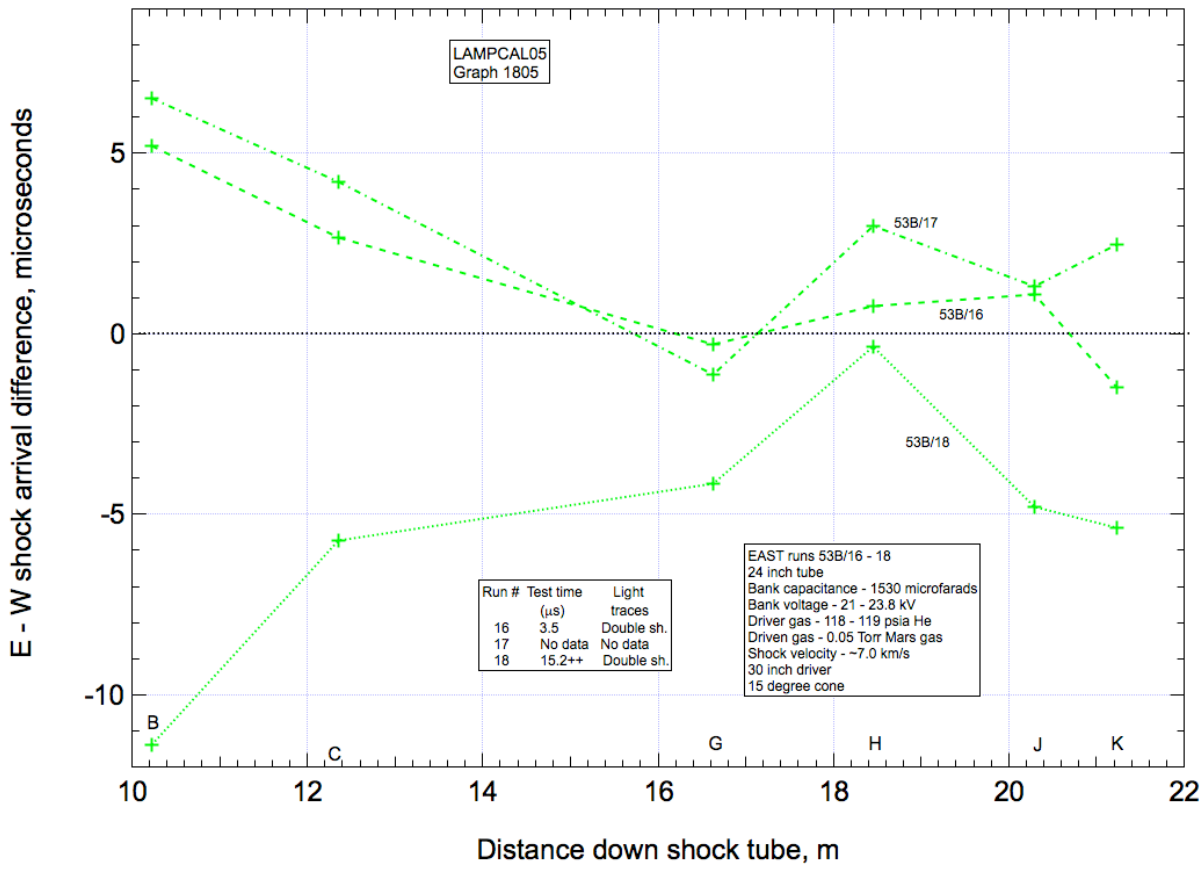

Figure 18. Shock wave tilt time delay versus distance along tube for Entry 53B. These data are from all tests in configuration (e), 30 inch driver with 15 degree cone (runs 16 - 18). Letters at bottom refer to diagnostic ports seen in Fig. 3.

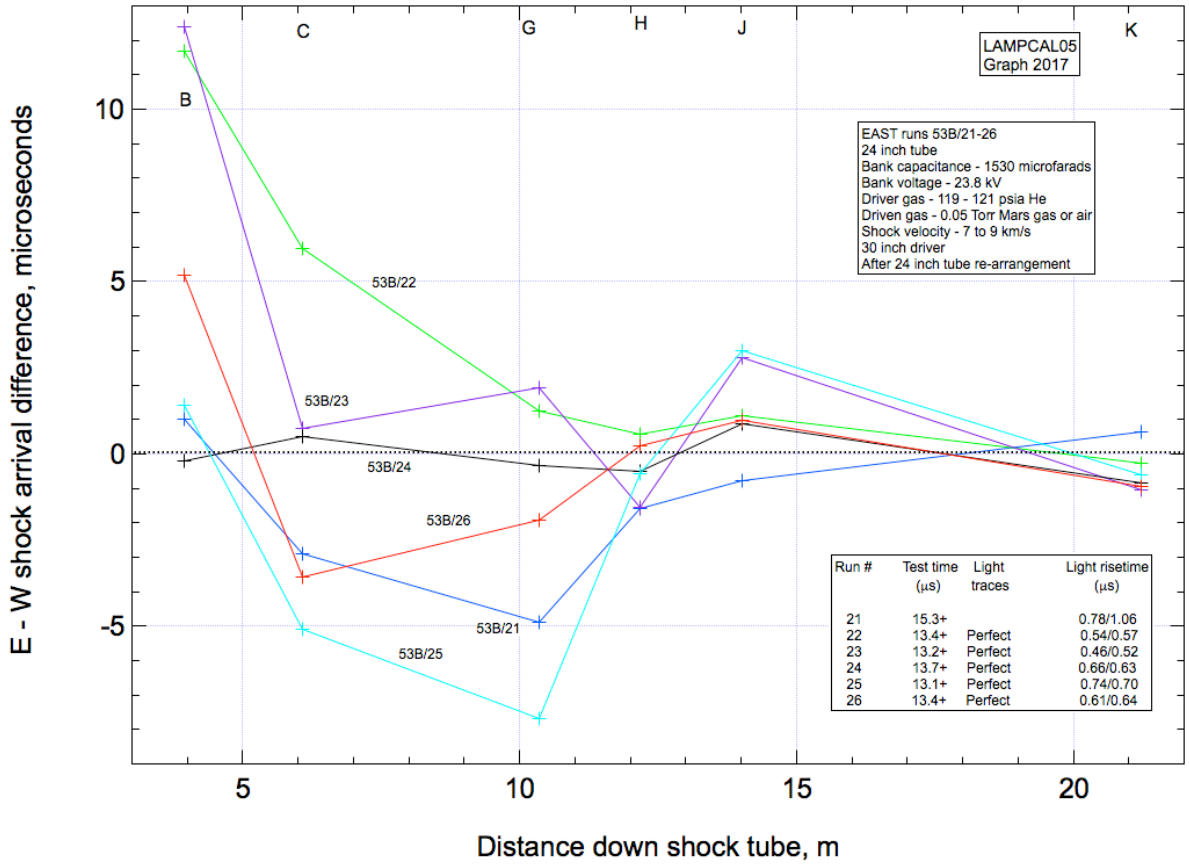

Figure 19. Shock wave tilt time delay versus distance along tube for Entry 53B. This includes data from all tests in configuration (g), with re-arranged tube sections (runs 21 - 26). Letters at bottom refer to diagnostic ports seen in Fig. 3.

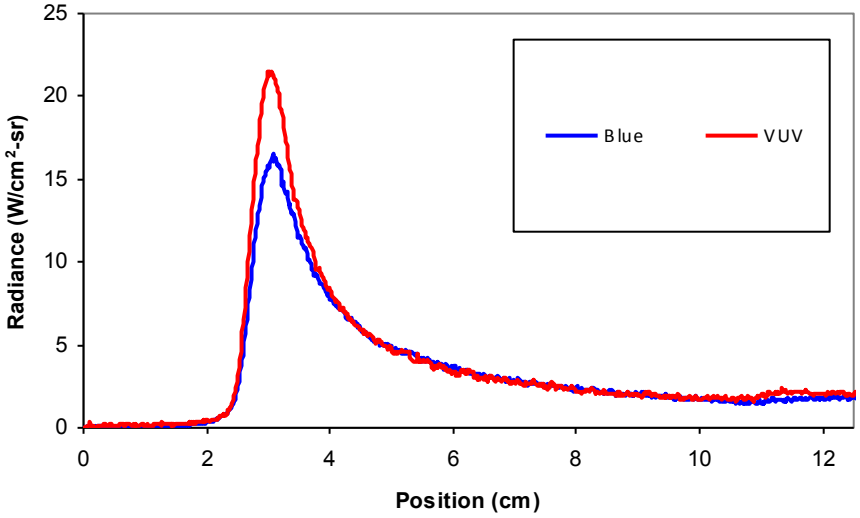

Figure 20. Light radiance versus distance along test section window for the two spectrometers. Entry 53B, run 10.

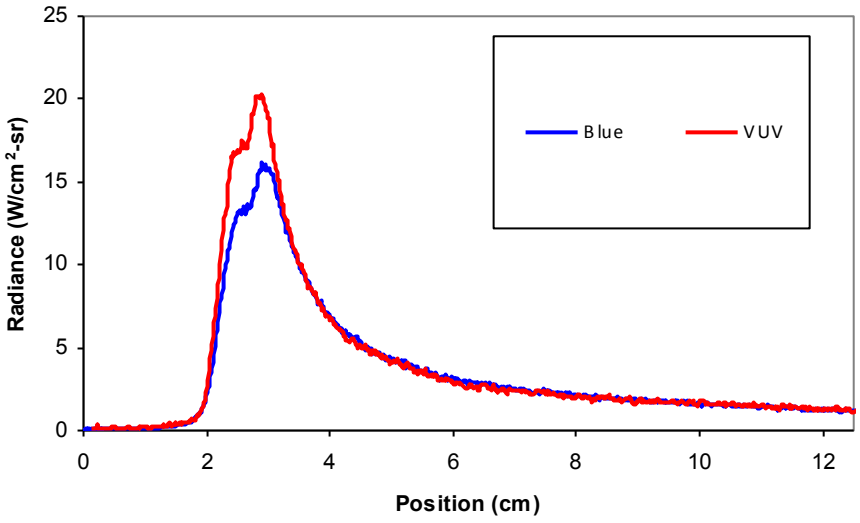

Figure 21. Light radiance versus distance along test section window for the two spectrometers. Entry 53B, run 11.

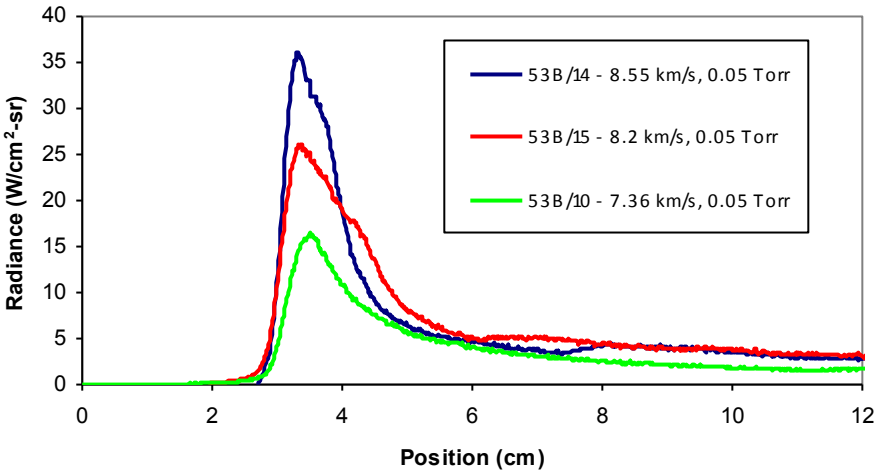

Figure 22. Blue spectrometer wavelength integrated light emission plotted versus imaged position for Entry 53B, runs 10, 14 and 15. See text for discussion.

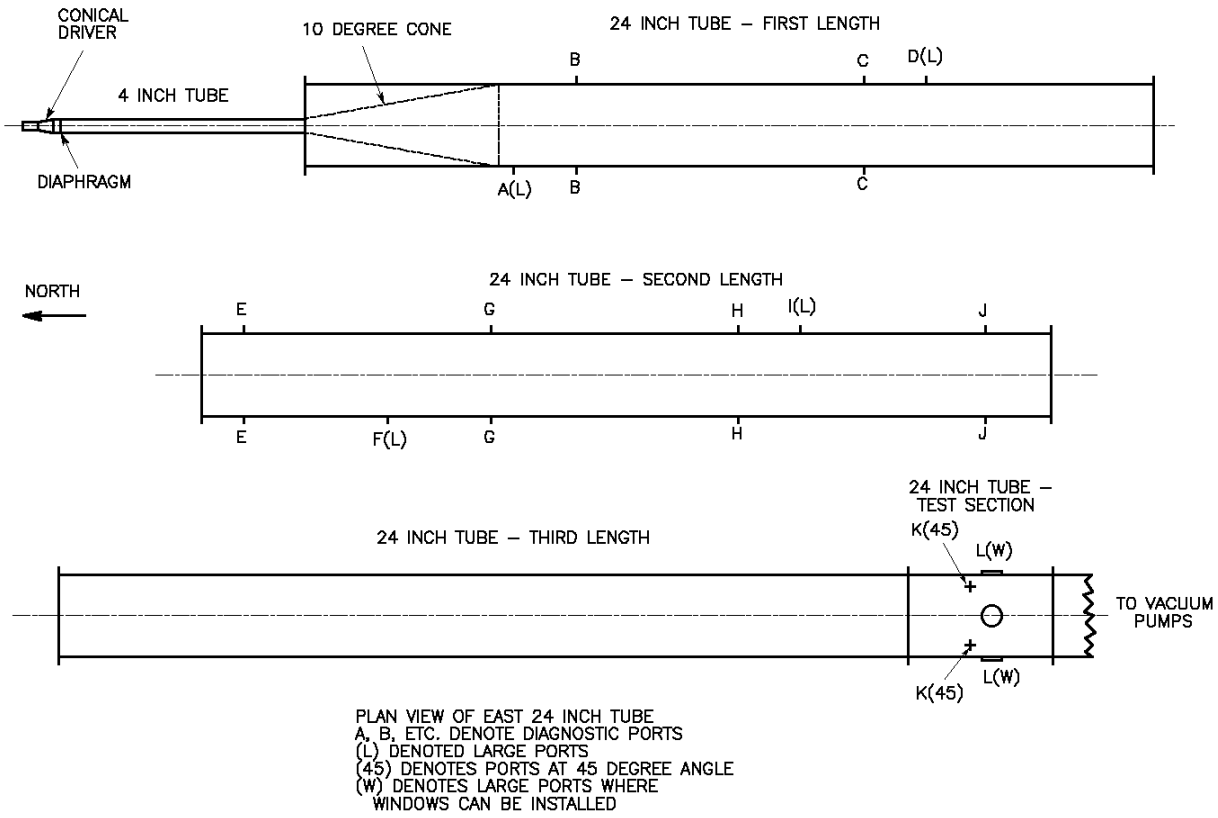

Figure 23. Schematic sketch of EAST 24 inch tube configuration shown in Fig. 6(g). This is an expanded version of Fig. 6(g), showing all diagnostic ports.

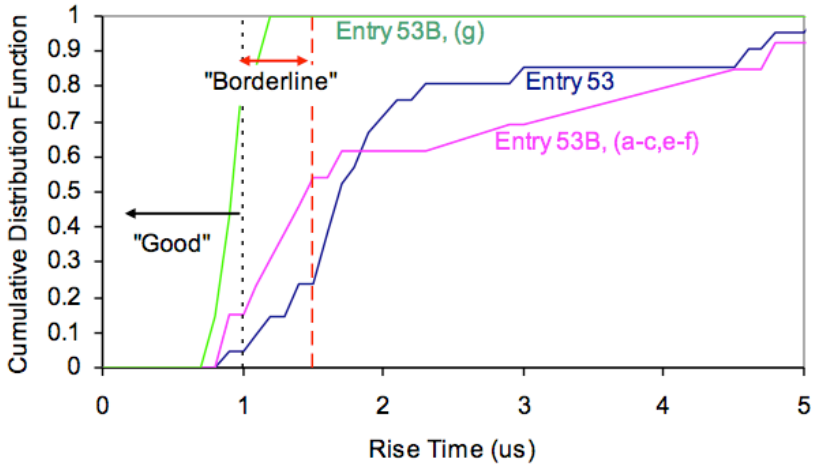

Figure 24. Fraction of different test series with rise times under the given value. Subjective criteria of 1 and 1.5 μs are shown as "good" and "borderline" limits.

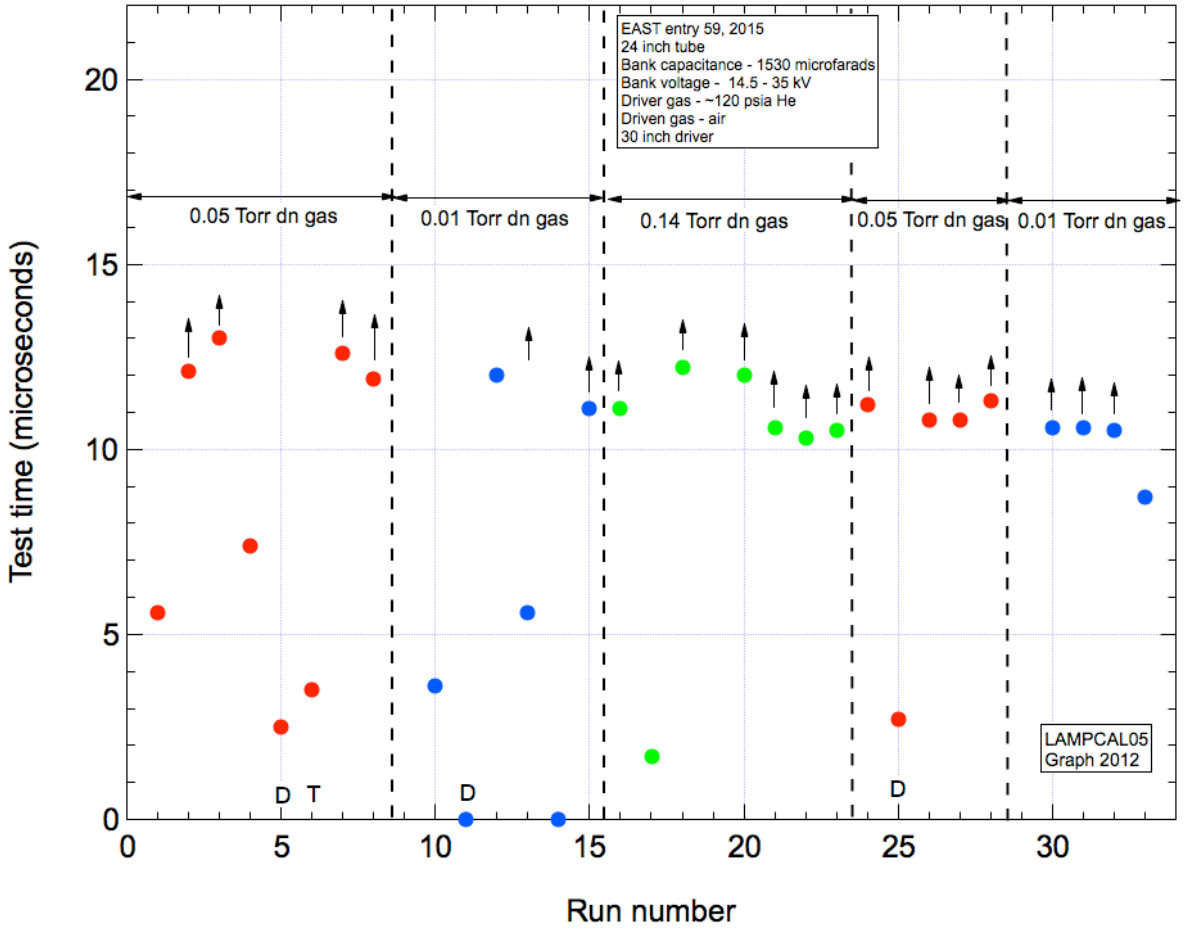

Figure 25. Test time versus run number for Entry 59. Arrows indicate that test times are equal to or exceed those indicated by the data points.

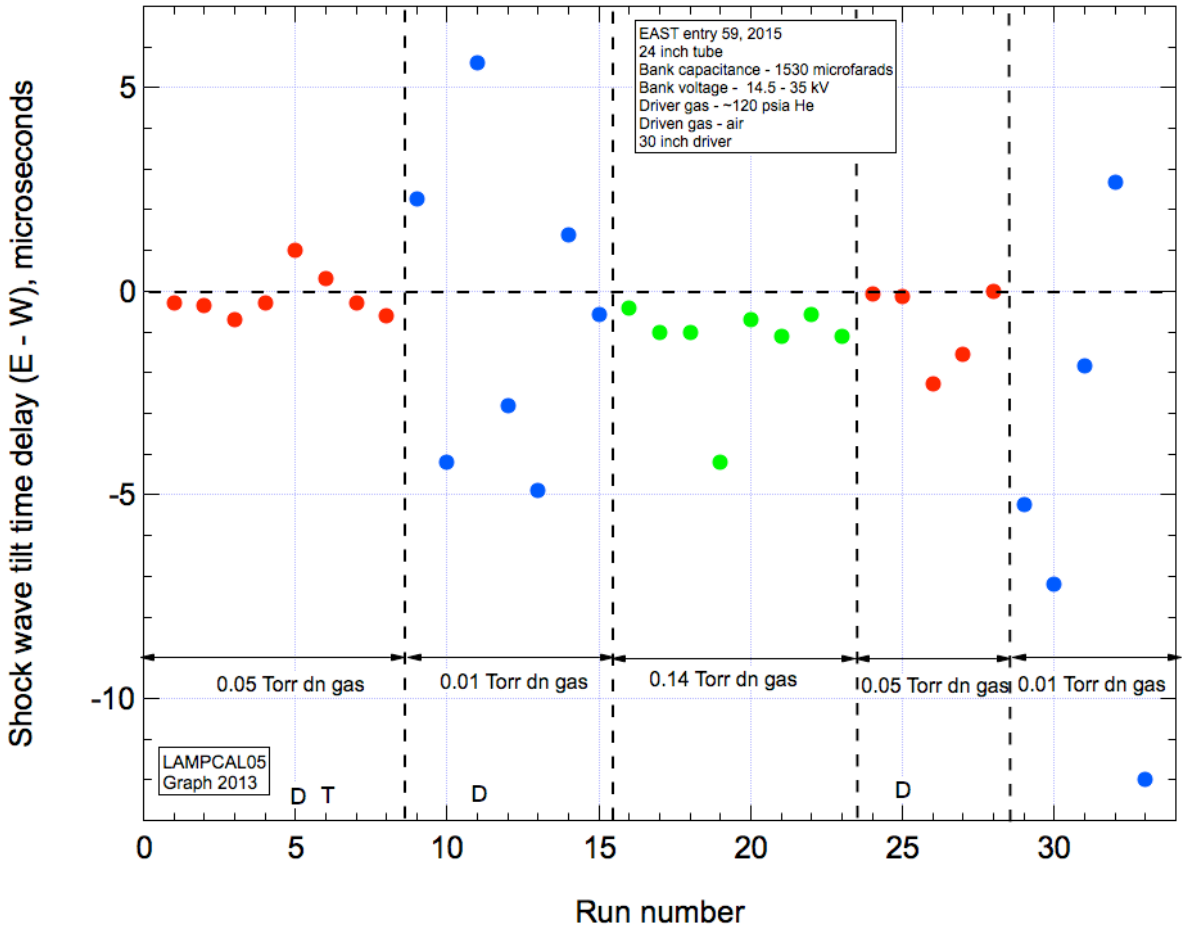

Figure 26. Shock wave tilt time delay versus run number for Entry 59.

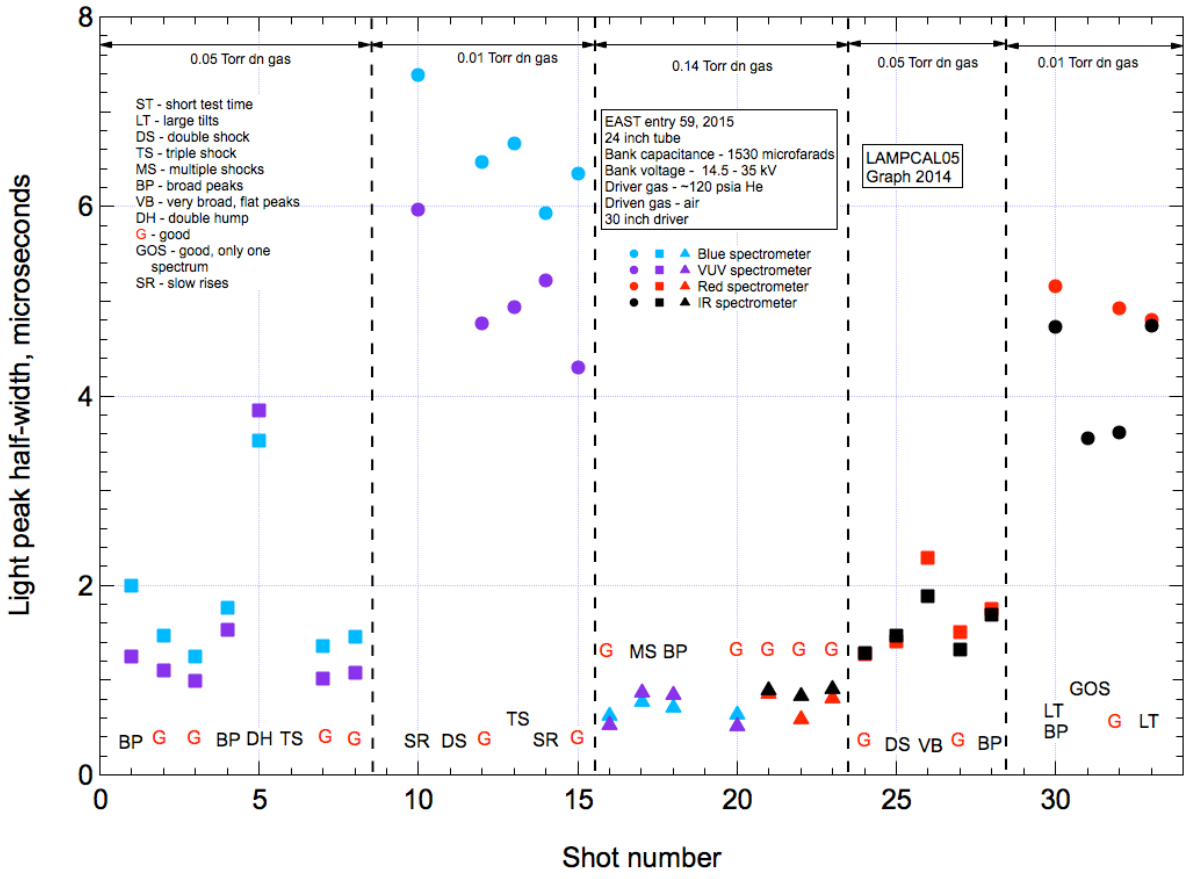

Figure 27. Half-widths of the spectrometer light peaks versus run number for Entry 59.

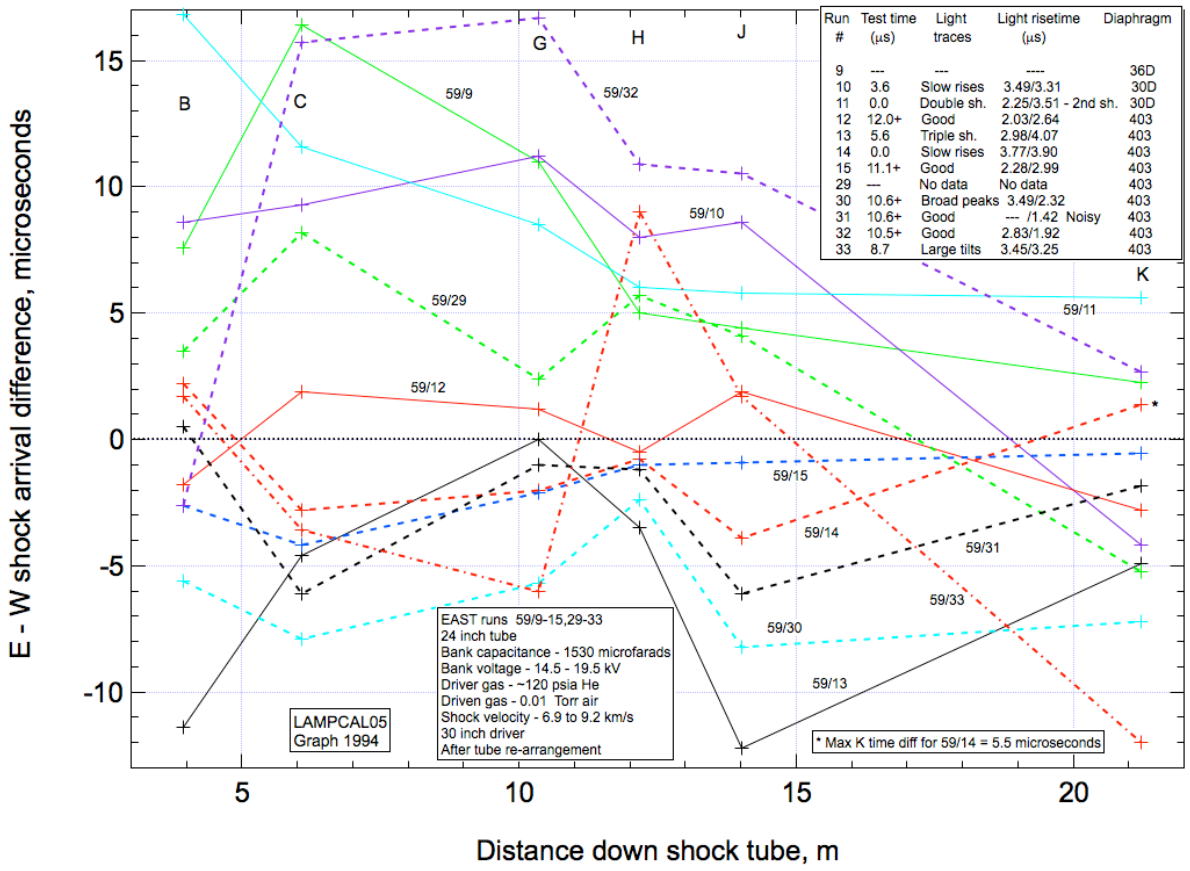

Figure 28. Shock wave tilt time delay versus distance along tube for Entry 59. Driven tube pressure is 0.01 Torr. Letters at top refer to diagnostic ports seen in Fig. 23.

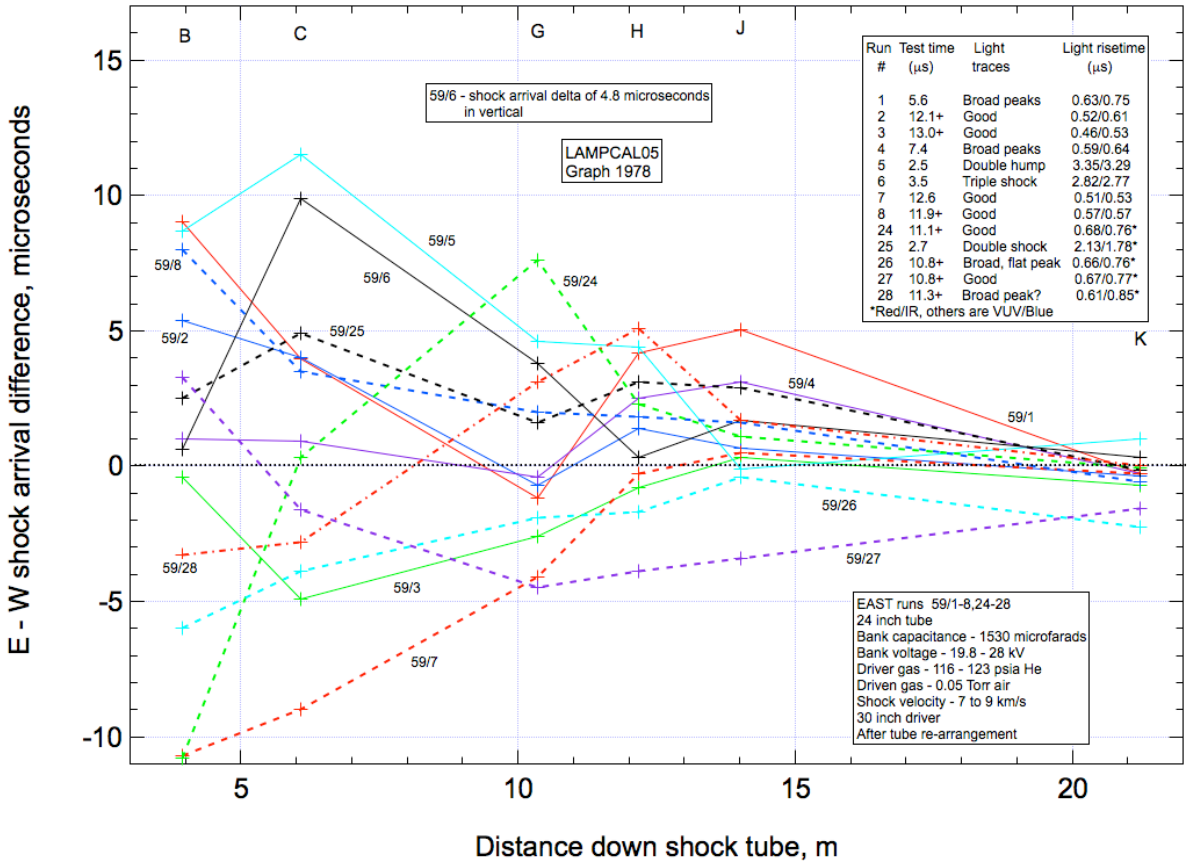

Figure 29. Shock wave tilt time delay versus distance along tube for Entry 59. Driven tube pressure is 0.05 Torr. Letters at top refer to diagnostic ports seen in Fig. 23.

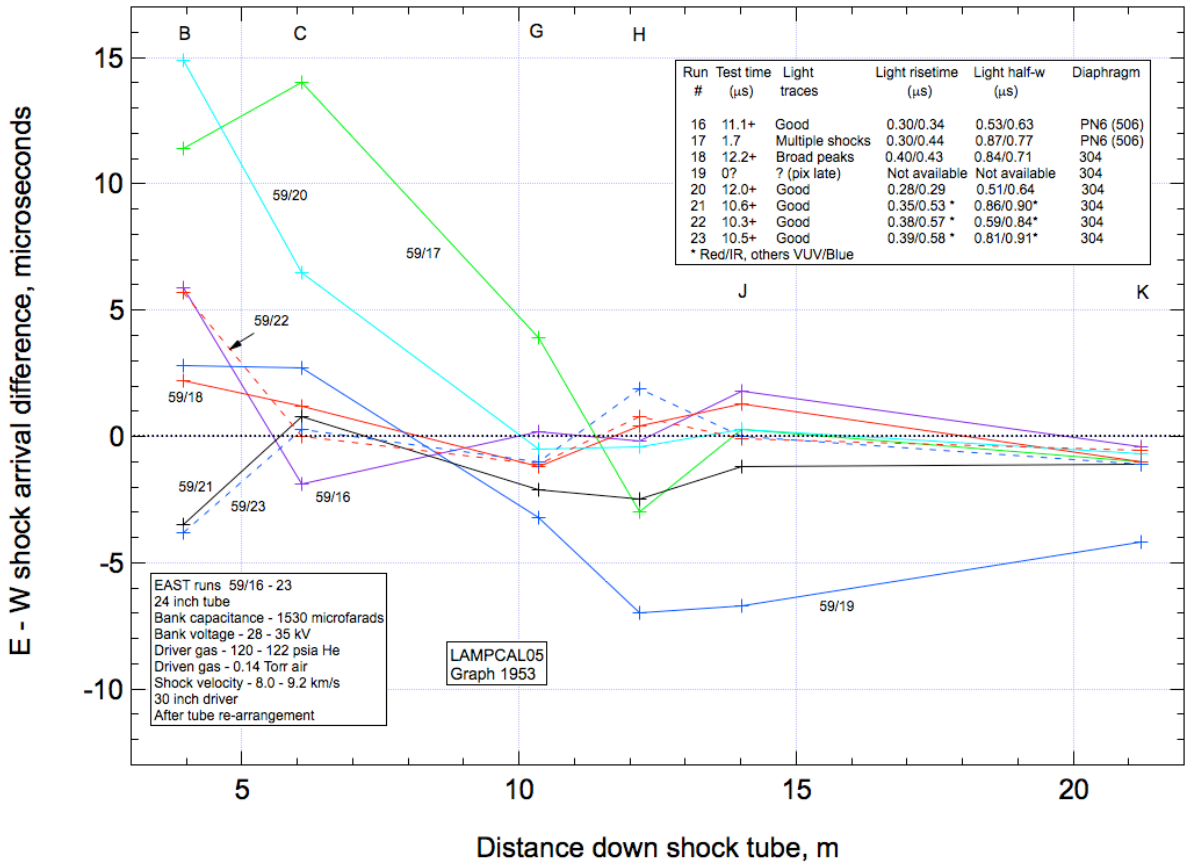

Figure 30. Shock wave tilt time delay versus distance along tube for Entry 59. Driven tube pressure is 0.14 Torr. Letters at top refer to diagnostic ports seen in Fig. 23.

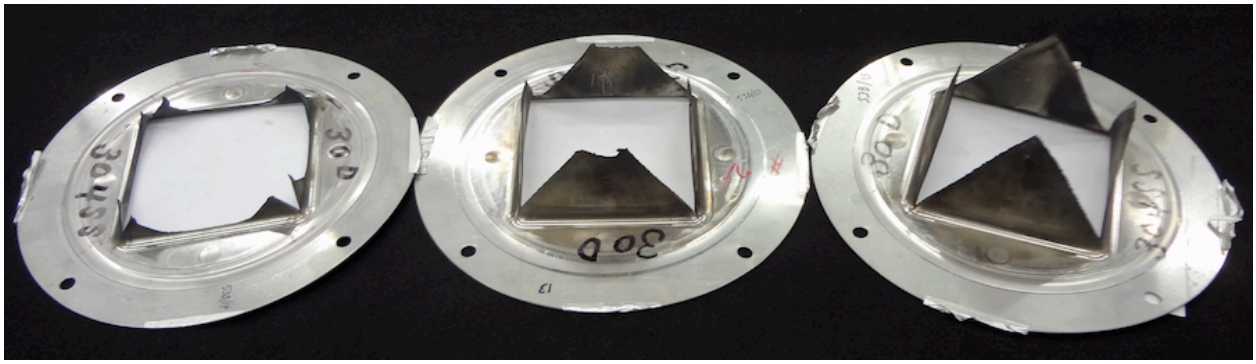

(a) (b) (c)

Figure 31. Ruptured diaphragms. (a) with whole petals thrown, (b) with petal tips thrown, (c) good diaphragm break.

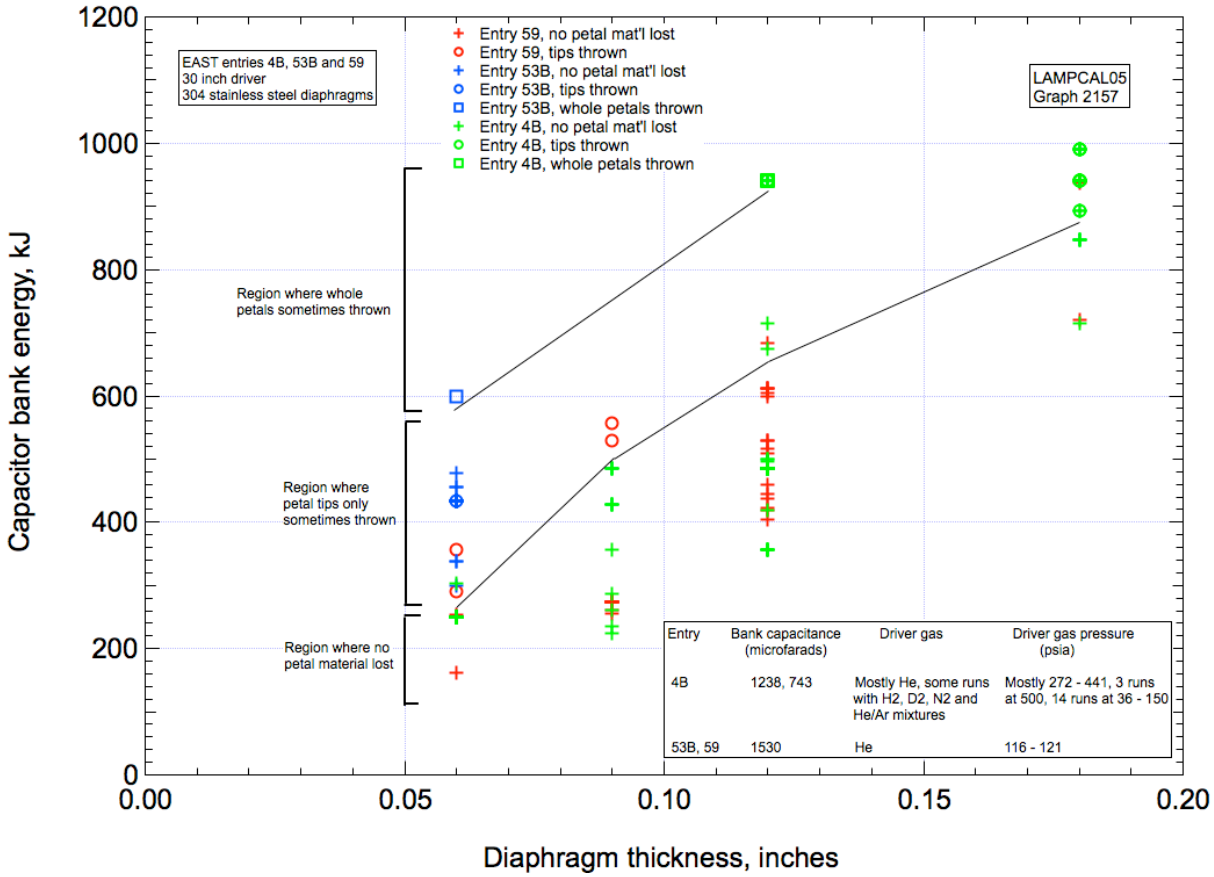

Figure 32. Capacitor bank energy versus diaphragm thickness for Entries 4B, 53B and 59. 30 inch driver. Inclined lines separate data points for various degrees of loss of diaphragm material.

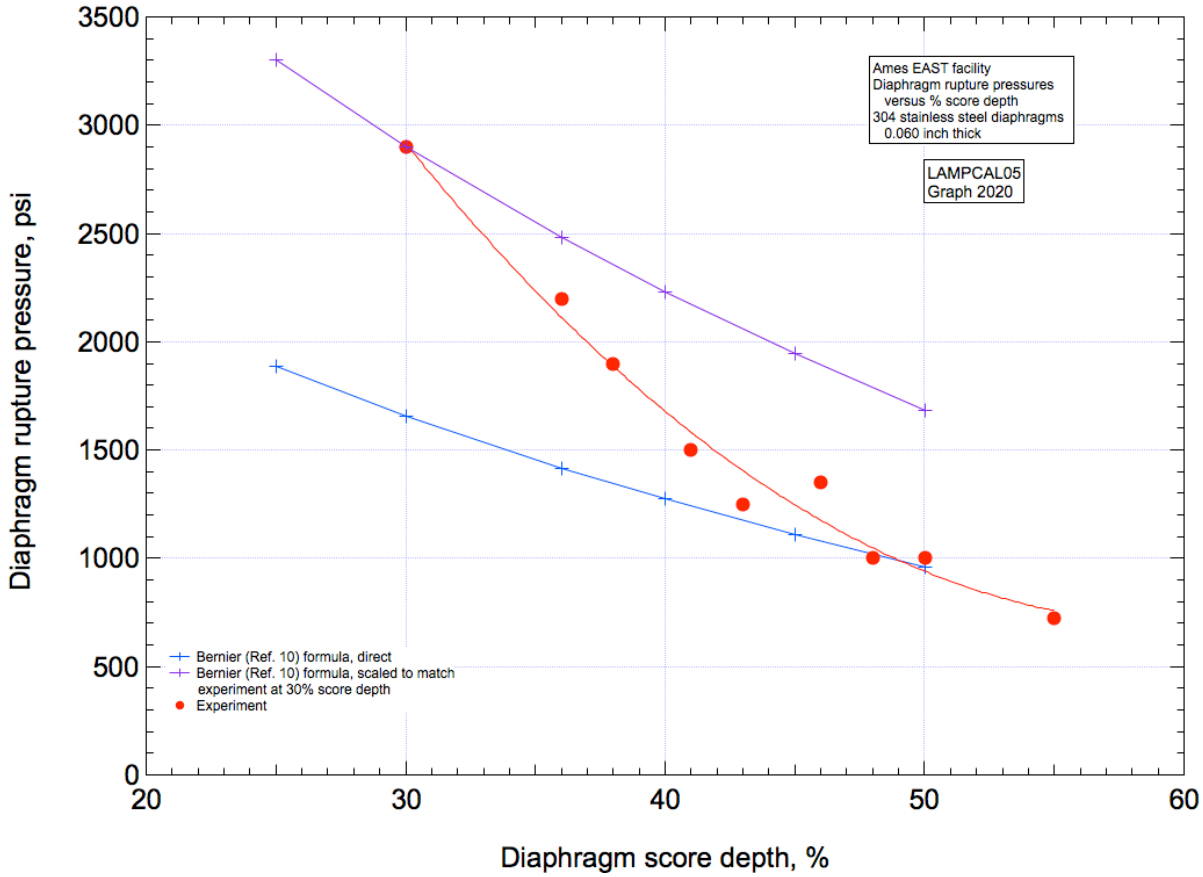

Figure 33. Diaphragm rupture pressure versus diaphragm score depth.

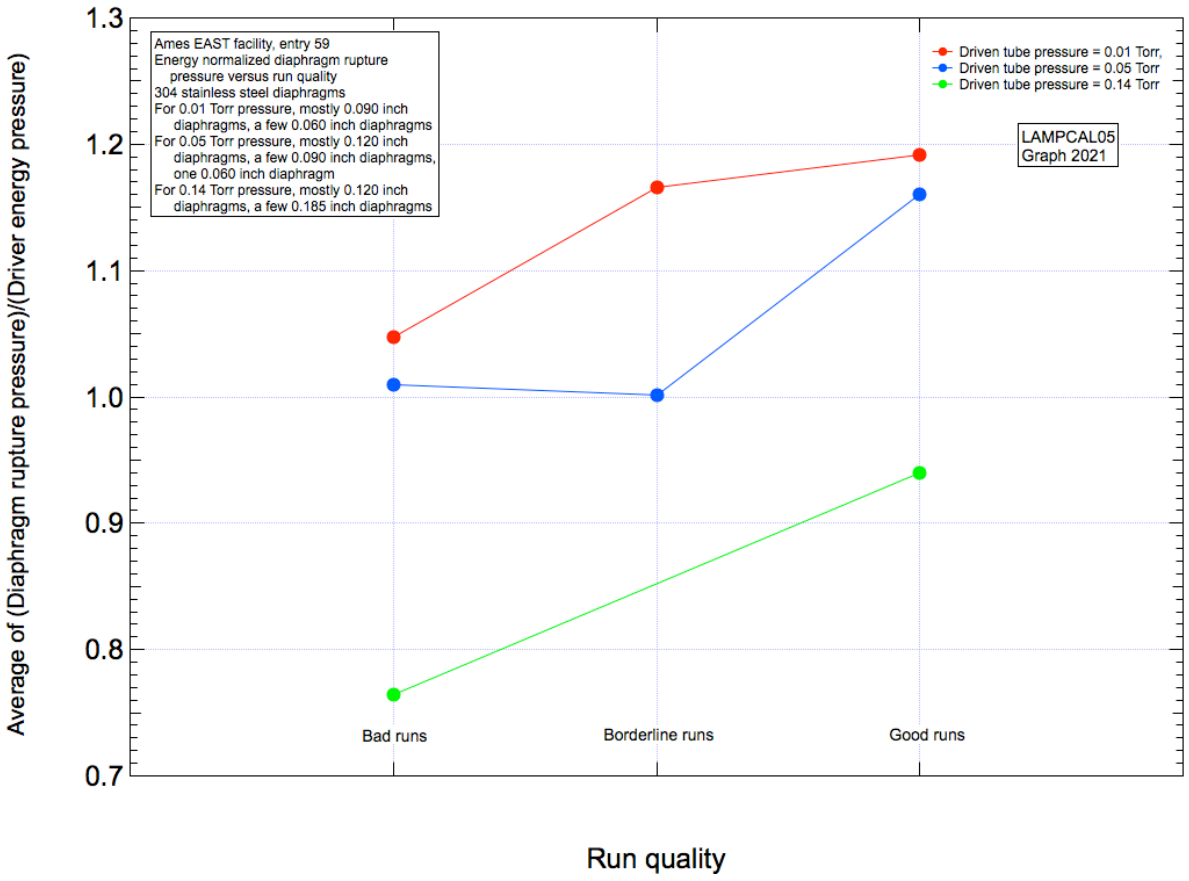

Figure 34. Average of diaphragm rupture pressure normalized by driver energy pressure versus run quality. Data for EAST Entry 59.